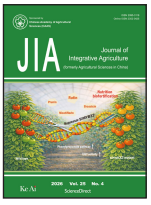
Journal of Integrative Agriculture 2026, 25(4): 1384–1401

Available online at ScienceDirect

Journal of Integrative Agriculture



RESEARCH ARTICLE

The mitochondrial genes *orf113b* and *orf146* from Xinjiang wild rapeseed cause pollen abortion in alloplasmic male sterility

Man Xing[1, 2], Bo Hong[1, 2], Chunyun Guan[1, 2, 3], Mei Guan[1, 2, 3#]

[1] *College of Agronomy, Hunan Agricultural University, Changsha 410128, China*
[2] *Hunan Branch of National Oilseed Crops Improvement Center, Changsha 410128, China*
[3] *Southern Regional Collaborative Innovation Center for Grain and Oil Crops in China, Changsha 410128, China*

Highlights

- First mitochondrial genome of Xinjiang wild rapeseed identifies two candidate sterility genes, *orf113b* and *orf146*.
- *orf113b* and *orf146* disrupt mitochondrial function, induce reactive oxygen species (ROS) accumulation, and lead to pollen abortion.
- ROS produced by *orf113b* and *orf146* mediates retrograde signaling to dysregulate nuclear genes essential for tapetum and microspore development.

Abstract

Nsa CMS is a type of cytoplasmic male sterility (CMS) in rapeseed that originated from the cross between Xinjiang wild rapeseed (*Sinapis arvensis*) and Xiangyou 15 (*Brassica napus* L.). Although this CMS variant shows promising applications, the factors contributing to its sterility and their underlying mechanisms remain unclear. To the best of our knowledge, we successfully assembled and analyzed the mitochondrial genome of 1258A (*Nsa* CMS) for the first time. This mitochondrial genome spans 263,010 bp and contains 91 genes, including 33 protein-coding and 36 *orf* genes. Our analysis identified a novel mitochondrial gene, *orf113b*, and a mutated, truncated gene, *orf146*, both likely linked to the sterility observed in 1258A. ORF113b and ORF146 were found to impede cell growth, disrupt gene expression associated with complexes I, III, and V of the mitochondrial oxidative phosphorylation pathway, and trigger reactive oxygen species (ROS) production. In addition, transcriptome data analysis revealed key nuclear genes co-expressed with *orf113b* and *orf146*, suggesting that their aberrant expression may be influenced by retrograde signaling from the mitochondria. This signaling could lead to atypical programmed cell death (PCD) in the tapetum layer, resulting in pollen sterility. In conclusion, our study not only provides the first characterization of the *Nsa* CMS mitochondrial genome but also identifies *orf113b* and *orf146* as crucial for pollen sterility. Furthermore, it suggests that the ROS induced by these mitochondrial genes may play a central role in the abnormal regulation of nuclear genes essential for pollen development, thus offering new insights into the molecular mechanisms underlying *Nsa* CMS.

Keywords: *Brassica napus* L., cytoplasmic male sterility, *orf113b*, *orf146*, reactive oxygen species (ROS)

1. Introduction

Cytoplasmic male sterility (CMS) is widely employed to develop and exploit hybrid vigor in rapeseed. The discovery and breeding of new sterile materials have expanded CMS types, enhancing the cytoplasmic genetic diversity in three-line hybrids of rapeseed. This diversification reduces the risks associated with the prolonged use of a single cytoplasm in seed production. Using distant hybridization technology, the female parent Xinjiang wild rapeseed (wild mustard, *Sinapis arvensis*) was crossed with the male parent Xiangyou 15 (XY15, *Brassica napus* L.) (Guan and Yin 2014). From this hybrid progeny, a rapeseed line with *Nsa* CMS, which was derived from Xinjiang wild rapeseed, was selected. Through years of selection across multiple generations, the sterile line 1258A was developed, and it exhibits complete pollen sterility and stable male sterility. This line shows significant potential

Received 9 June 2024; Received in revised form 20 August 2024; Accepted 11 September 2024; Available online 24 September 2024
Man Xing, E-mail: xingman18971@outlook.com; #Correspondence Mei Guan, E-mail: guanmei@hunau.edu.cn

© 2026 CAAS. Publishing services by Elsevier B.V. on behalf of KeAi Communications Co. Ltd. This is an open access article under the CC BY-NC-ND license (http://creativecommons.org/licenses/by-nc-nd/4.0/). Peer review under responsibility of Editorial Board of *Journal of Integrative Agriculture*.
doi: 10.1016/j.jia.2024.09.018

for widespread application in harnessing hybrid vigor in rapeseed.

The first *Nsa* CMS was generated through somatic hybridization between Zhongshuang 4 (*B. napus* L.) and *S. arvensis*, with *orf346* being identified as its mitochondrial male sterility gene (Hu *et al.* 2002; Liu *et al.* 2015; Sang *et al.* 2021). Research on Xinjiang wild rapeseed spanning over 30 years has established that it is not a new species but rather *S. arvensis* (Guan 1996). Consequently, two types of *B. napus Nsa* CMS lines have been developed: one *via* somatic fusion technology (Hu *et al.* 2002; Liu *et al.* 2015; Sang *et al.* 2019) and the other through distant hybridization (Guan and Yin 2014; Xing *et al.* 2022). Both lines trace their cytoplasmic origin to Xinjiang wild rapeseed. Although the sterility mechanism of *Nsa* CMS has been partially elucidated with the identification of *orf346*, further research is required to fully understand the sterility mechanisms in other *Nsa* CMS lines.

Mitochondrial genes previously implicated in CMS within the Brassicaceae family include *orf138* (*Ogu* CMS) (Singh *et al.* 2021), *orf125* (*Kosena* CMS) (Iwabuchi *et al.* 1999), *orf72* (*mur* CMS) (Shinada *et al.* 2006), *orf224* (*pol* CMS) (Wang *et al.* 1995), *orf222* (*Nap* CMS) (Li *et al.* 2020), *orf288* (*hau* CMS) (Heng *et al.* 2018), *orf263* (*tournefortii* CMS) (Landgren *et al.* 1996), *orf220* (*tubermustard* CMS) (Yang *et al.* 2010), and *orf346* (*Nsa* CMS) (Sang *et al.* 2021). A notable feature of these sterility genes is their chimeric structure, indicating the fusion of sequences from different genes. For instance, *orf288* in *hau* CMS contains a sequence from *nad5* (Heng *et al.* 2018), while *orf222* in *Nap* CMS and *orf224* in *pol* CMS are chimeric with the mitochondrial gene *atp8* (Handa *et al.* 1995; L'Homme *et al.* 1997). Similarly, *orf346* in *Nsa* CMS exhibits high homology to the 5′ end of *cox1* and is co-transcribed with *nad3* and *rps12* (Sang *et al.* 2021). The CMS mechanism has been extensively studied in various species, including rice (Kazama *et al.* 2016; Takatsuka *et al.* 2022), maize (Xiao *et al.* 2020; Yang *et al.* 2022), wheat (Melonek *et al.* 2021), cotton (You *et al.* 2022; Zhang *et al.* 2022, 2023), rapeseed (L'Homme *et al.* 1997; Du *et al.* 2019), tomato (Kuwabara *et al.* 2022), chili pepper (Wen *et al.* 2021; Nikornpun *et al.* 2023), and tobacco (Wang *et al.* 2020; Dewey *et al.* 2023). This phenomenon is typically linked to mitochondrial DNA rearrangements, the emergence of novel open reading frames (ORFs), or chimeric ORFs. However, the correlation between these genetic factors and the CMS phenotype is not always direct. Some ORFs associated with CMS are hypothetical, as variations in them do not consistently correlate with the CMS phenotype, and the case of radish *Ogu* CMS exemplifies this complexity (Chase 2007; Chen and Liu 2014). In *Ogu* CMS, extensive mitochondrial genome recombination and rearrangement result in the sterile gene *orf138*, which is not clearly chimeric (Singh *et al.* 2021). This genetic diversity in CMS underscores the complexity of the mechanism. While chimeric mitochondrial genes are commonly identified in CMS sterility genes, there is no definitive evidence that such chimeric genes are essential for inducing pollen sterility through CMS.

Reactive oxygen species (ROS) are crucial in plant cell signal transduction and homeostasis, as they significantly influence stress responses and reproductive development. The occurrence of CMS is often linked to ROS accumulation in anthers. ROS can signal the induction of programmed cell death (PCD) in tapetum cells (Mittler *et al.* 2022; Ge *et al.* 2025). In rice CMS-HL, the CMS protein ORFH79 binds to complex III, causing mitochondrial dysfunction, oxidative stress, reduced ATP levels, and increased ROS content. These changes, along with interactions between mitochondrial retrograde signals like ROS and nuclear genes, contribute to pollen abortion (Wang *et al.* 2013). Similarly, the mitochondrial *orf355* gene in maize CMS-S and the chimeric *atp6c* gene in maize CMS-C trigger ROS bursts which lead to premature PCD in tapetum cells and result in maize CMS (Xiao *et al.* 2020; Yang *et al.* 2022). Studies in wheat (Wang *et al.* 2022), cotton (Zhang *et al.* 2022), rapeseed (Shang *et al.* 2021), and other CMS types have shown that mitochondrial sterile genes cause excessive ROS accumulation in anthers, a key factor in pollen abortion. Transcripts or proteins from rearranged mitochondrial sterile genes may directly impair mitochondrial gene function or induce ROS bursts at specific stages *via* interacting proteins, ultimately leading to abnormal PCD in the tapetum and CMS development.

In this study, we explored the roles of the cytoplasmic mitochondrial genes *orf113b* and *orf146*, derived from Xinjiang wild rapeseed, in regulating pollen sterility. By assembling and annotating the mitochondrial genomes of 1258A and 1258B, both originating from Xinjiang wild rapeseed, we identified two key genes involved in CMS. The expression of *orf113b* and *orf146* alters mitochondrial gene expression and oxidative phosphorylation, leading to increased mitochondrial ROS content and reduced ATP levels, which are crucial factors in pollen sterility induction. The expression of these genes in *Arabidopsis thaliana* also triggers a defense response and significantly upregulates certain nuclear genes, highlighting the complex interplay between mitochondrial and nuclear genomes in plant fertility. Therefore, these findings offer new insights into the molecular mechanisms underlying rapeseed CMS and provide a theoretical basis for advancing the practical application of the *Nsa* CMS system.

2. Materials and methods

2.1. Plant materials

Academician Chunyun Guan developed *Nsa* CMS through distant hybridization using Xinjiang wild rapeseed (*S. arvensis*) as the maternal parent and Xiangyou 15 (XY15) as the paternal parent (Guan and Yin 2014). The *Nsa* CMS materials included 1258A and its maintainer line, 1258B, both sourced from the Oil Crops Research Institute of Hunan Agricultural University (Changsha, China). These plant materials were cultivated at Hunan Agricultural University's "Yunyuan" Experimental Field in Changsha, Hunan, from September 2021 to May 2022.

2.2. RNA extraction, RT-PCR and quantitative real-time PCR

During the full flowering stage of rapeseed, flower buds of 1258A and 1258B (flower bud size≤2 mm) were harvested. The tetrad stage of pollen development within the flower bud

marks the early stage of pollen abortion in 1258A (Xing *et al.* 2022). Using sterilized tweezers, the anthers were quickly removed from the peeled open flower buds and immediately frozen in liquid nitrogen. Total RNA was extracted from the anthers using the Plant Total RNA Rapid Extraction Kit (Sangon Biotech Shanghai Co., Ltd., China) following the manual's instructions. cDNA synthesis was carried out using the One-Step gDNA Removal and cDNA Synthesis SuperMix (TransGen Biotech Co., Ltd., Beijing, China) with the cDNA obtained from the reverse transcription of 1258A and 1258B as templates. RT-PCR amplification was then performed using the primers listed in Appendix A. The PCR reaction system included 1 μL template, 1 μL forward primer, 1 μL reverse primer, 10 μL 2×Phanta Flash Master Mix, and 7 μL ddH_2O. The PCR program comprised 94°C for 3 min, followed by 35 cycles of 94°C for 30 s, 60°C for 30 s, and 72°C for 90 s, with a final extension at 72°C for 10 min. The target bands were detected through 1% agarose gel electrophoresis. In the qRT-PCR analysis, *B. napus Actin2.1* served as the internal reference gene, with the primers listed in Appendix A. Relative expression levels were calculated using the method described by Livak and Schmittgen (2001).

2.3. Transcriptome sequencing of transgenic *A. thaliana*

Arabidopsis thaliana inflorescences were initially flash frozen with liquid nitrogen and stored at –80°C until testing. Three biological replicates were prepared for each treatment. RNA was extracted from the inflorescences using the TRIzol method and subjected to purity and integrity testing. The NEBNext Ultra RNA Library Prep Kit (New England Biolabs Co., Ltd., Beijing, China) was used to construct the library. After construction, the library was preliminarily quantified using the Qubit 2.0 fluorometer and diluted to 1.5 ng μL^{-1}. The library insert size was then checked using an Agilent 2100 bioanalyzer. If the insert size met expectations, the library's effective concentration was accurately quantified *via* qRT-PCR to ensure a concentration higher than 2 nmol L^{-1}, thereby ensuring library quality. Sequencing was performed on the Illumina high-throughput sequencing platform (HiSeq2000). Differentially expressed genes (DEGs) were identified based on the screening criteria of $|\log_2(\text{Fold Change})| \geq 1$ and $q < 0.05$. These DEGs were then functionally annotated and analyzed based on the Gene Ontology (GO) and Kyoto Encyclopedia of Genes and Genomes (KEGG) databases.

2.4. Mitochondrial gene extraction, sequencing and assembly

The seeds of 1258A and 1258B were sown in nutrient pots and incubated at 25°C in a plant incubator under dark conditions for a week. Etiolated seedlings, each weighing 5 g, were harvested, flash frozen with liquid nitrogen, and stored at –80°C. Mitochondria were isolated and purified from the etiolated seedlings using the method described by Eubel *et al.* (2006), involving differential centrifugation and discontinuous Percoll gradients (40, 28, and 15%). Mitochondrial DNA was extracted using the QIAamp DNA Mini Kit (QIAGEN Co., Ltd., Shanghai, China). The total amount of DNA was measured with fluorescent dye (Quant-iT PicoGreen dsDNA Assay Kit (Thermo Fisher Scientific Co., Ltd., Shanghai, China)) and its integrity was checked through 1% agarose gel electrophoresis. The diluted DNA working solution was stored at 4°C, and the storage solution was stored at –20°C. For genome sequencing, the whole genome shotgun (WGS) strategy was used to construct libraries with different insert fragments. These libraries were sequenced using second-generation sequencing technology (Next-Generation Sequencing, NGS) based on the Illumina Novaseq sequencing platform and third-generation single-molecule sequencing technology based on the PacBio sequencing platform.

Mitochondrial genome assembly was initiated with the use of GetOrganelle v1.7.1 to assemble the Illumina sequencing data. Second-generation assembly sequences were aligned to the PacBio third-generation data using BWA v0.7.17. The target sample's third-generation data was extracted and hybrid assembled with the second-generation data using SPAdes v3.14.1. Sequences with high coverage depth and longer assembly length were selected. The mitochondrial scaffold sequences were verified by alignment to the NT database and connected based on overlap. The clean reads were mapped back to the mitochondrial genome sequence, and bases were corrected using Pilon v1.23. Finally, the starting position and orientation of the mitochondrial scaffold were determined based on the reference genome (JF920286.1) to obtain the final mitochondrial genome sequence.

Raw reads of the rapeseed accessions generated in this article can be accessed in the public database of the National Center of Biotechnology Information under BioProject accession PRJNA1100170. Sequence data from this article can be accessed in the GenBank database under accession numbers PP663684 and PP663685.

2.5. Mitochondrial functional component analysis

The tRNAscan-SE v2.0.7 software was used for predicting non-coding RNAs (ncRNAs) in the genome. In sample genomes, gene prediction was performed using a homology alignment prediction method. First, the protein sequences of the NCBI mitochondrial reference genome were rapidly aligned to the sample genome using BLAST+ 2.7.1 with a threshold–e value of 1e–5. Poor alignment results were filtered out, and redundancy was removed. The integrity of sample genes and exon/intron boundaries were manually corrected to obtain a highly accurate set of conserved genes.

2.6. KEGG annotation of protein-coding genes and genomic circle map

The KEGG Orthology (KO) of protein-coding genes primarily employs the KAAS (ver. 2.1) Automated Annotation System, which focuses on "Prokaryotes" and uses the bi-directional best hit (BBH) rule for gene KO determination. After annotation, KOs were mapped onto the corresponding KEGG pathways. The genomic circular map is primarily used to visualize genomes with circular structures and is commonly applied in initial genome studies to present basic genomic research results. Using OGDRAW software

(https://chlorobox.mpimp-golm.mpg.de/OGDraw.html) and the prediction results of coding genes, the 1258A and 1258B genomes were displayed in circular maps based on the assembled genome sequences.

2.7. Mitochondrial genome collinearity analysis and repeat sequence analysis

The mitochondrial genome sequence of *S. arvensis* (NC_031896.1) was downloaded for alignment. The starting sequences of the other two genomes were adjusted to match this reference. Then, Mauve (version 2.3.1) was used to align the 1258A genome with the reference genome.

The mitochondrial genome repeats, including random and tandem sequences, were analyzed. Forward, reverse, and palindromic repeat sequences in the genome were identified using bibiserv2 online (https://bibiserv.cebitec.uni-bielefeld.de/sessionTimeout.jsf). Tandem repeat analysis was performed using The Tandem Repeats Finder Server (https://tandem.bu.edu/trf/trf.html). The MAFFT online service (https://mafft.cbrc.jp/alignment/server/) was used for Dotter plot analysis to determine rearrangements.

2.8. Expression of the *orf113b* and *orf146* genes in *Escherichia coli* and yeast

First, the transmembrane structural domains of ORF113b and ORF146 amino acids were predicted using an online tool (https://services.healthtech.dtu.dk/services/TMHMM-2.0/). Gene-specific regions were amplified using primers (Appendix B), and the PCR products were cloned into *Eco*RI-*Hin*dIII digested pET28A and *Kpn*I-*Bam*HI digested pYES2 vectors. The recombinant products were transformed into the *E. coli* (Rosetta, DE3) and *Saccharomyces cerevisiae* (INVSc1) strains, respectively.

Protein induction expression analysis in *E. coli*: A single colony was cultured in 100 mL of Luria-Bertani (LB) medium with kanamycin (Kan; 50 mg L^{-1}) at 37°C and 180 r min^{-1} shaking for 6 h, until the OD_{600} reached 0.2. The culture was then divided into two equal parts. Isopropyl-β-D-thiogalactopyranoside (IPTG) was added to one part to a final concentration of 1 mmol L^{-1} for induction, while the other part served as the control. The culture was further incubated at 37°C with continuous shaking to induce protein expression, with monitoring of the OD value at regular intervals.

Protein induction expression analysis in yeast: A single colony was selected and inoculated into 100 mL of SC-Ura medium with Kan (50 mg L^{-1}) at 29°C and 220 r min^{-1} shaking until the OD_{600} reached 0.4. The culture was then divided equally into two parts. One part was supplemented with 2% Glu, and the other with 2% Gal. The culture was shaken at 29°C to induce protein expression, with the OD value measured at regular intervals. Once the OD_{600} reached 1, the culture was diluted in ten-fold serial dilutions and grown on SC-Ura+2% Glu and SC-Ura+2% Gal agar plates for 48 h.

2.9. ROS detection

The intracellular oxidation levels in *E. coli* were detected with the Reactive Oxygen Species Assay Kit from Beijing Solarbio Science & Technology Co., Ltd. (CA1410). Cultured *E. coli*, transformed with *orf113b* and *orf146*, were incubated at 37°C for 6 h until the OD_{600} reached 0.2. IPTG was then added to a final concentration of 1 mmol L^{-1} to stimulate gene expression. After 4 h of induction, 2 mL of the culture was collected and centrifuged at 3,000×g to isolate the bacteria. These were then resuspended in the fluorescent probe from the ROS assay kit. Simultaneously, Rosup was added to *E. coli* transformed with the empty vector pET28A at a final concentration of 5 μmol L^{-1} to induce a significant level of ROS. After a 30 min incubation at 37°C, the cells were washed twice with PBS buffer, and ROS content changes were observed under a laser confocal microscope at 488 nm.

2.10. Construction of plant expression vectors and genetic transformation

For the mitochondrial targeting sequence, the first 1–165 bp sequence of the rapeseed restorer gene *Rfo* (LOC108827691) was used. Following Sang *et al.* (2021), *orf113b* and *orf146* were fused with this mitochondrial targeting sequence to yield *MTS:orf113b* and *MTS:orf146*. The *AP3* (*APETALA3*) promoter was inserted into the PC2300 (pCAMBIA2300) vector, and *MTS:orf113b* and *MTS:orf146* were subsequently introduced into the vector. The *orf113b* and *orf146* genes were placed under the control of the *CaMV35S* promoter in the PC1300S vector. The primer sequences used for gene cloning are listed in Appendix C. Then, the constructed vectors were transformed into *Agrobacterium tumefaciens* GV3101, and the target genes were transferred into *A. thaliana via* the floral dip method.

2.11. Hydrogen peroxide (H_2O_2) stress test

The rapeseed seeds were sown on filter paper in a Petri dish to maintain the necessary moisture for germination. They were grown in a plant growth chamber for 5 d, by which time the roots had grown to 1 cm in length. The seedlings were then transferred to Petri dishes treated with H_2O_2 (20 mmol L^{-1}) and distilled water, respectively. After a 6 h exposure, the expression of mitochondrial oxidative phosphorylation genes and the ATP content in the seedlings were measured. The ATP Content Assay Kit was purchased from Sangon Biotech (Shanghai) Co., Ltd., and used according to the manufacturer's instructions.

3. Results

3.1. Sequencing, *de novo* assembly, and general features of the 1258A and 1258B mitochondrial genomes

We employed Illumina and PacBio Sequel II technologies to sequence the mitochondrial genome. The DNA sample was sequenced using Illumina NovaSeq 6000 technology in a paired-end manner. After quality control processing, the effective data volumes (clean data) for the 1258A and 1258B samples were 7,900.3 and 7,632.1 Mb, with Q_{20} values of 96.66 and 96.87%, and Q_{30} values of 88.65 and 89.25%, respectively. The average GC content of the effective data was 40.25% for 1258A and 40.04% for 1258B (Appendix D). The Illumina sequencing data were assembled using GetOrganelle v1.7.1. The PacBio Sequel II sequencing data, after filtering, yielded 483,630,402 and 84,042,273

total bases for samples 1258A and 1258B, respectively. The number of reads was 54,583 for 1258A and 9,663 for 1258B. The longest subread length for 1258A was 175,173 bp with an average of 8,860 bp, while for 1258B, these values were 175,555 and 8,697 bp, respectively. Finally, the starting positions and orientations of the mitochondrial scaffolds were determined based on the reference genome, resulting in the mitochondrial genome sequences for 1258A and 1258B being 263,010 and 262,916 bp long, respectively (Appendix E).

Based on the assembled genome sequences of 1258A and 1258B, along with the predicted coding genes, the genomes were illustrated in circular diagrams (Fig. 1-A and B). In 1258A, 91 genes were identified, comprising three ribosomal RNAs (rRNAs), 19 transfer RNAs (tRNAs), 36 *orf* genes, and 33 protein-coding genes. In contrast, 1258B contains 100 genes, including three rRNAs, 29 tRNAs, 35 *orf* genes, and 33 protein-coding genes. The lower number of non-coding RNAs in 1258A compared to 1258B is attributed to the 10 fewer tRNAs in 1258A (Appendix F). The 33 protein-coding genes could be categorized into 10 functional groups: ATP synthase (*atp1*, *atp4*, *atp6*, *atp8*, and *atp9*), cytochrome c biogenesis (*ccmB*, *ccmC*, *ccmFC*, *ccmFN1*, and *ccmFN2*), ubiquinol cytochrome c reductase (*cob*), cytochrome c oxidase (*cox1*, *cox2*, and *cox3*), maturases (*matR*), transport membrane protein (*tatC*), NADH dehydrogenase (*nad1*, *nad2*, *nad3*, *nad4*, *nad4L*, *nad5*, *nad6*, *nad7*, and *nad9*), large ribosomal subunit (*rpl2*, *rpl5*, and *rpl16*), small ribosomal subunit (*rps3*, *rps4*, *rps7*, *rps12*, and *rps14*), and ribosomal RNAs (*rrn5*, *rrn18*, and *rrn26*) (Appendix F). The KEGG annotation results for the two mitochondrial protein-coding genes in both genomes are identical, with *atp1*, *atp6*, *atp9*, *cob*, *cox1*, *cox2*, *cox3*, *nad1*, *nad2*, *nad3*, *nad4*, *nad5*, *nad6*, *nad7*, and *nad9* being annotated in the metabolic pathways, oxidative phosphorylation, and thermogenesis pathways (Fig. 1-C). The genes examined are implicated in mitochondrial oxidative phosphorylation (OXPHOS) and electron transfer, which are both essential for energy metabolism. Annotation of the ORFs revealed that 1258A contains four unique ORF genes — *orf108a*, *orf113b*, *orf117a*, and *orf147* — while 1258B has three — *orf101d*, *orf123*, and *orf164* (Fig. 1-E). An analysis of dispersed repetitive sequences identified two types in the mitochondrial genome: direct repeats and inverted repeats. The mitochondrial genome of 1258A comprises 59 direct and 41 inverted repeats, totaling 12,243 bp and representing 4.65% of the genome. In contrast, 1258B contains 47 direct and 53 inverted repeats, totaling 10,850 bp and accounting for 4.13% of its genome (Fig. 1-D). The most frequent repetitive sequences were 30–39 bp in length, followed by 40–49 bp sequences, with only two exceeding 1 kb (Fig. 1-D).

3.2. Genomic evidence suggests that the 1258A mitochondrial genome originated from Xinjiang wild rapeseed

Although 1258A and 1258B were selected from the progeny of distant hybridization between Xinjiang wild rapeseed and Xiangyou 15, their mitochondrial genomes are significantly larger — 1258A (263,010 bp) and 1258B (262,916 bp) — than the *S. arvensis* mitochondrial genome (240,024 bp). To explore the origins of their mitochondrial genomes, we conducted a Dotter plot analysis using the MAFFT online service (https://mafft.cbrc.jp/alignment/server/) to identify rearrangements. As depicted in Fig. 2-A–C, extensive co-linear regions exist between the mitochondrial genomes of 1258A, 1258B, and *S. arvensis*. While the nucleotide sequences within these regions are highly conserved, the arrangement and orientation of the co-linear regions have undergone evolutionary rearrangements, indicating that 1258A may have evolved different cytoplasmic types. We compared the phylogenetic relationships of the mitochondrial genomes at the nucleotide level through average nucleotide identity (ANI) analysis. The results showed that 1258A and 1258B share the highest homology at 99.92%, while 1258A and *S. arvensis* exhibit 99.27% homology, and 1258B and *S. arvensis* show 99.32% homology (Appendix G). This high level of homology confirms that both the male sterile line and its maintainer line (derived from distant hybridization offspring of Xinjiang wild rapeseed) possess mitochondrial genomes originating from Xinjiang wild rapeseed.

To elucidate the structural composition of the mitochondrial genome, we conducted a collinearity analysis using Mauve visualization technology. This analysis revealed a high degree of collinearity between the mitochondrial genomes of 1258A, 1258B, and *S. arvensis*, as evidenced by numerous homologous blocks (Fig. 2-D). Utilizing the known sequences of 19 mitochondrial genomes from *Brassicaceae* plants (Appendix H), we employed MEGA7 software to assess the phylogenetic relationships between the 1258A and 1258B genomes and those of other species. The results showed that the 1258A and 1258B mitochondrial genomes are distantly related to the reported rapeseed mitochondrial genomes, and they form distinct clusters. Notably, 1258A clustered exclusively with *S. arvensis*, indicating a close relationship and forming a separate branch (Appendix I). Therefore, these findings suggest that the mitochondrial genome of 1258A is distinct from the reported rapeseed mitochondrial genomes and likely originated from Xinjiang wild rapeseed (*S. arvensis*).

3.3. Screening of CMS-related genes in the mitochondrial genome

Although the origin and evolution of new mitochondrial genes, including plant CMS genes, and their functional acquisition remain enigmatic, they are generally linked to specific *orf*s in the mitochondrial genome (Tang *et al.* 2016). In this study, we performed sequence alignment and transmembrane domain analysis on all the *orf*s and protein-coding genes of 1258A and 1258B. Our findings revealed base deletions and mutations in the mitochondrial gene 1258A *orf146* (the *orf146* gene in this article refers to the CMS mitochondrial gene unless specified otherwise) compared to its counterpart in 1258B. Specifically, the full length of 1258B *orf146* is 441 bp, whereas 1258A *orf146* is 402 bp. Within the *cox3-ccmFC* region, a 39 bp deletion in 1258A *orf146* resulted in a reduced transmembrane domain, thus altering the amino acid sequence and type (Fig. 3-A). In addition, single base mutations at positions 210, 320, and 324 bp, along

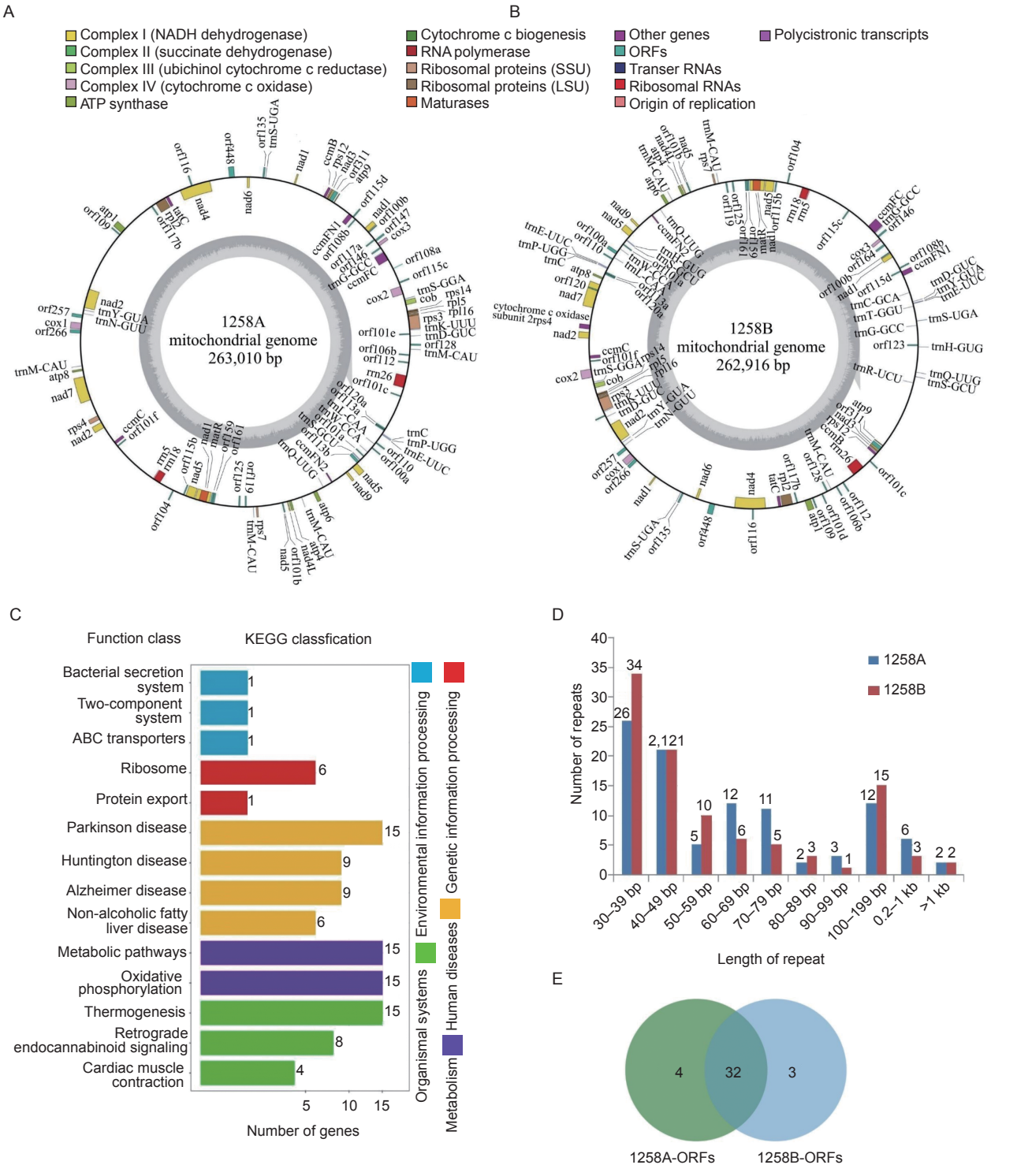


Fig. 1 Mitochondrial genome annotation and comparative analysis of 1258A and 1258B. A and B, complete mitochondrial genome maps of 1258A and 1258B. C, Kyoto Encyclopedia of Genes and Genomes (KEGG) functional annotation and statistics of protein-coding genes. D, 1258A and 1258B mitochondrial genome repeat sequence statistics. E, Venn diagram counts of open reading frames (ORFs) in 1258A and 1258B.

with a base deletion at 315 bp in 1258A *orf146*, directly affected the amino acid sequence, resulting in the loss of a transmembrane domain in 1258A ORF146 (Fig. 3-B). These mutations and deletions are likely to affect gene function, so we consider 1258A *orf146* a candidate CMS gene. Furthermore, among the four mitochondrial genes unique to 1258A, only *orf113b* encodes an amino acid sequence with two transmembrane domains (Fig. 3-D). Most identified CMS genes result from mitochondrial genome rearrangements, typically involving chimeric ORFs that encode transmembrane proteins (Menassa *et al.* 1999; Luo *et al.* 2013; Chen and Liu 2014). Therefore, we propose that *orf113b*, a mitochondrial

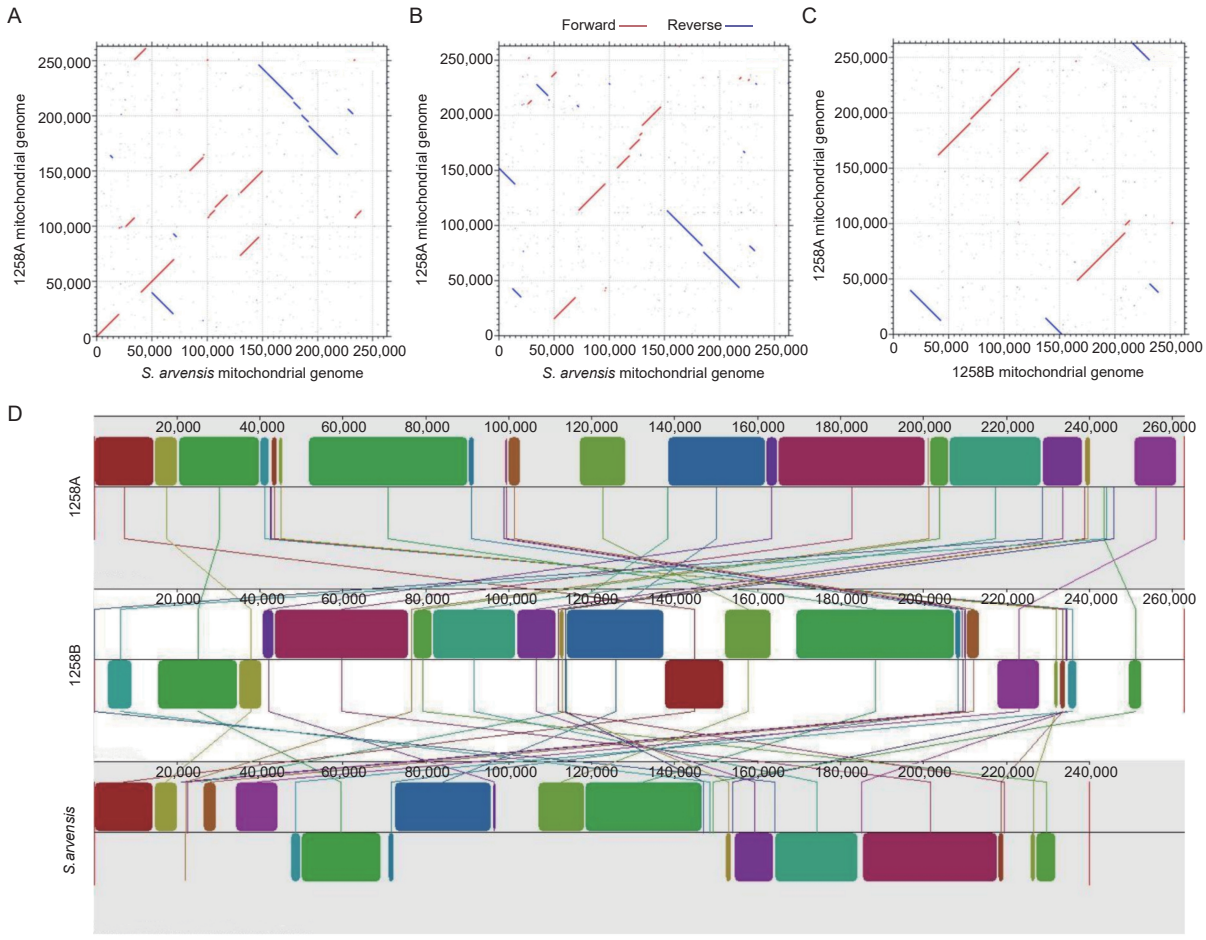


Fig. 2 Comparative analysis of the mitochondrial genomes. A and B are dot plot graphs showing the collinearity between the mitochondrial genomes of 1258A and 1258B with that of *S. arvensis*. C, dot plot graph showing the collinearity between the mitochondrial genomes of 1258A and 1258B. D, identification of collinear segments of the mitochondrial genomes of 1258A and 1258B with *Sinapis arvensis* using the Mauve visualization technology. The lines connecting two gene blocks indicate the high homology between those two gene blocks.

gene unique to 1258A with transmembrane domains, is a strong candidate for causing CMS. Structural analysis of the *orf113b* gene in mitochondria revealed that in the corresponding mitochondrial regions of both 1258A and 1258B, a base deletion occurred at 483 bp accompanied by 13 base mutations. This led to the production of a 729 bp *orf113b* gene in the mitochondrial genome of 1258A (Fig. 3-E). Similarly, a 117 bp deletion in the *nad1-cox3* region altered the *orf164* gene sequence, resulting in the production of two unique genes in 1258A, *orf117a* and *orf147*; however, neither encodes transmembrane proteins (Appendix J).

We analyzed the expression of eight *orf*s in the flower buds of 1258A and 1258B using RT-PCR. Six of the eight genes were expressed in both the sterile line (1258A) and the maintainer line (1258B), except for *orf113b* and *orf146*, which were detected only in 1258A. However, a trace amount of expression of *orf146* was also observed in 1258B (Fig. 3-F). We then amplified the full-length sequences of *orf113b* and *orf146* from 1258A, 1258B, and XY15. While *orf113b* was exclusively amplified from 1258A, *orf146* was amplified from all three samples, although the band was faint in XY15 (Fig. 3-G). Abortive CMS genes are typically specific to sterile cytoplasm. *orf113b*, which is uniquely expressed in the sterile line, contains a transmembrane domain and exhibits characteristics of CMS-associated abortive genes. The variation in 1258A *orf146*, resulting from sequence deletion and base mutation which leads to the loss of transmembrane domains and changes in amino acid composition, may induce functional changes, highlighting the distinct nature of sterile cytoplasm genes. Consequently, *orf113b* and *orf146* were identified as high-potential candidate genes related to CMS.

3.4. The *orf113b* and *orf146* genes inhibit growth in *E. coli* and yeast

To study the functions of the *orf113b* and *orf146* genes, we performed heterologous expression in both prokaryotic (*E. coli*) and eukaryotic (yeast) systems. Following IPTG induction, *orf113b* and *orf146* significantly inhibited *E. coli* growth, which eventually recovered as indicated by an increase in OD values over time. Notably, *orf146* from strain 1258B also inhibited *E. coli* growth after induction; however, this inhibition was transient (Fig. 4-A), and the growth curve soon aligned with that of the IPTG-induced empty vector. This transient inhibition may be due to the shared amino acid sequence and transmembrane domain between 1258B

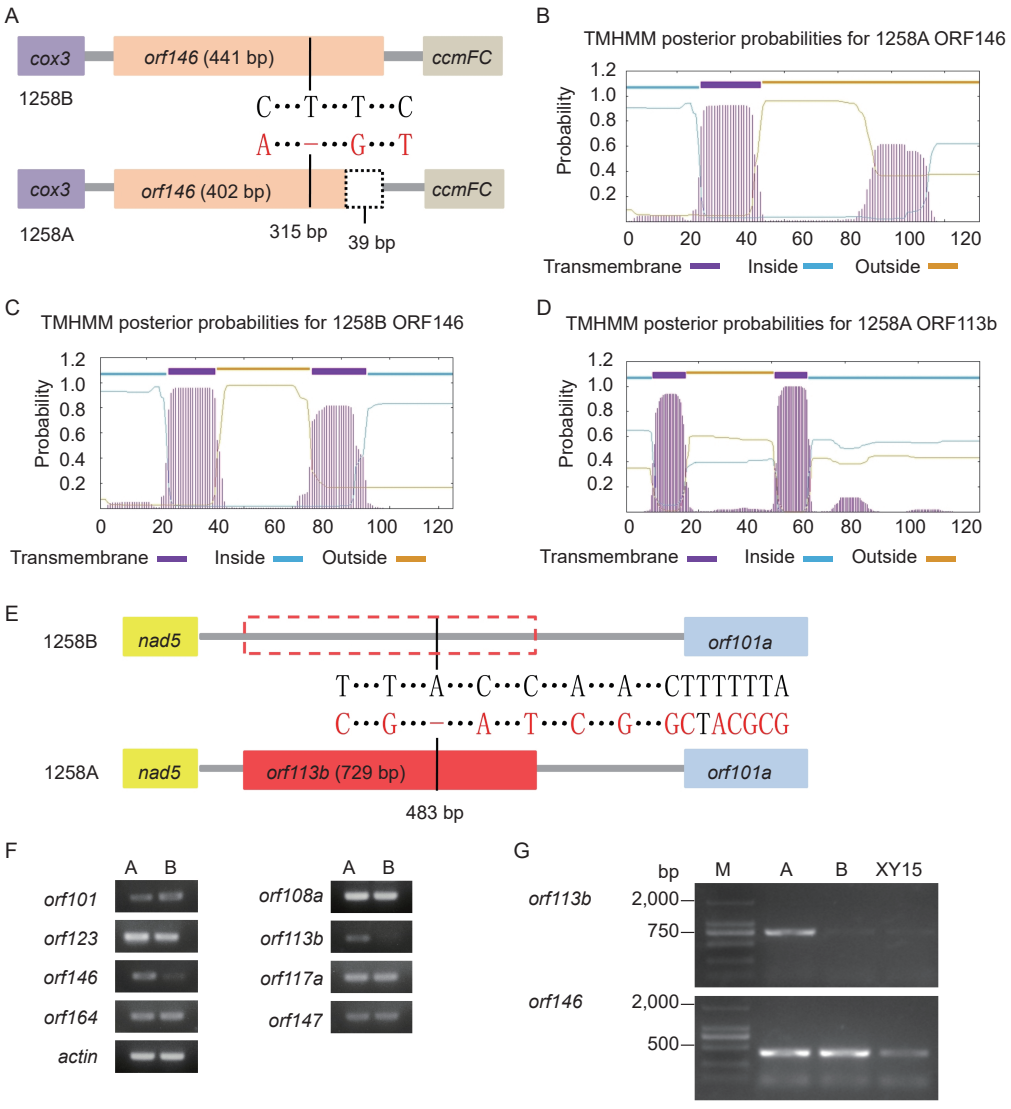


Fig. 3 *orf113b* and *orf146* gene structure schematics and semiquantitative analysis of the differential mitochondrial genes. A, schematic diagram of the mitochondrial genome structure of the *orf146* gene in 1258A and 1258B, with dashed boxes indicating regions with base deletions. B, analysis of the ORF146 transmembrane domain in 1258A, which features one transmembrane domain. C, analysis of the ORF146 transmembrane domain in 1258B, which features two transmembrane domains. D, analysis of the ORF113b transmembrane domain in 1258A, which features two transmembrane domains. E, schematic diagram of the mitochondrial genome structure of the *orf113b* gene in 1258A and 1258B, with dashed boxes indicating regions with base deletions and mutations. F, RT-PCR analysis of the eight differential mitochondrial genes. G, gene amplification results of *orf113b* and *orf146* in 1258A, 1258B, and Xiangyou 15, showing amplification only in 1258A. M, DNA marker; A, 1258A; B, 1258B; XY15, Xiangyou 15.

ORF146 and 1258A ORF146, despite the absence of a transmembrane domain in 1258A ORF146, which leads to functional divergence. In yeast, the inhibitory effect was even less pronounced. The growth curves of 1258A *orf146* and 1258B *orf146* nearly overlapped after induction, and the differences in growth between *orf113b*- and *orf146*-induced yeast, and the empty vector were minimal (Fig. 4-B). On Glu growth medium plates, transgenic yeast expressing *orf113b* and *orf146* showed viability that was consistent with yeast transformed with the empty vector. Although cell vitality decreased on Gal induction medium plates, the differences among the various transgenic yeast strains were insignificant (Fig. 4-C). Thus, *orf113b* and *orf146* exhibited a stronger inhibitory effect on prokaryotic cell activity compared to eukaryotic cells. To determine whether this inhibition is related to the transmembrane domain, ORF113b was truncated and expressed in *E. coli* (Fig. 4-D). The results revealed that only the truncated protein containing the transmembrane domain inhibited *E. coli* growth (Fig. 4-E), underscoring the importance of the transmembrane domain in the function of this sterility gene.

3.5. *orf113b* and *orf146* induce a ROS burst by regulating the expression of OXPHOS genes

Based on the inhibitory effects observed in *E. coli* and yeast cells, we hypothesize that the expression of the *orf113b* and *orf146* genes may affect mitochondrial gene function. To investigate this hypothesis, we extracted

RNA from 1258A and 1258B anthers at the pollen tetrad stage and performed qRT-PCR analysis on 15 annotated mitochondrial OXPHOS genes. The analysis revealed that in the mitochondrial complex I of 1258A, *nad1*, *nad2*, *nad3*, and *nad5* were significantly upregulated, while the complex III gene (*cob*), complex IV genes (*cox1* and *cox3*), and complex V genes (*atp1*, *atp6*, and *atp9*) were significantly downregulated (Fig. 5-A). The five enzyme complexes in the electron transport chain (ETC) that support OXPHOS — complex I (NADH, ubiquinone oxidoreductase), complex II (succinate dehydrogenase, SDH), complex III (cytochrome bc1 oxidoreductase), complex IV (cytochrome c oxidase), and complex V (ATP synthase) — are critical for mitochondrial function. The differential expression of these mitochondrial enzyme complex genes in 1258A suggests a potential disruption of ETC function, which may impact key biological processes, including ROS production (Vercellino and Sazanov 2021). To further examine this mechanism, we confirmed in *E. coli* that *orf113b* and *orf146* gene expression stimulated excessive ROS production (Fig. 5-B). Following IPTG-induced expression of these genes, we observed fluorescence signals under a laser confocal microscope that were like those seen under the ROS inducer Rosup in the empty vector (Fig. 5-B).

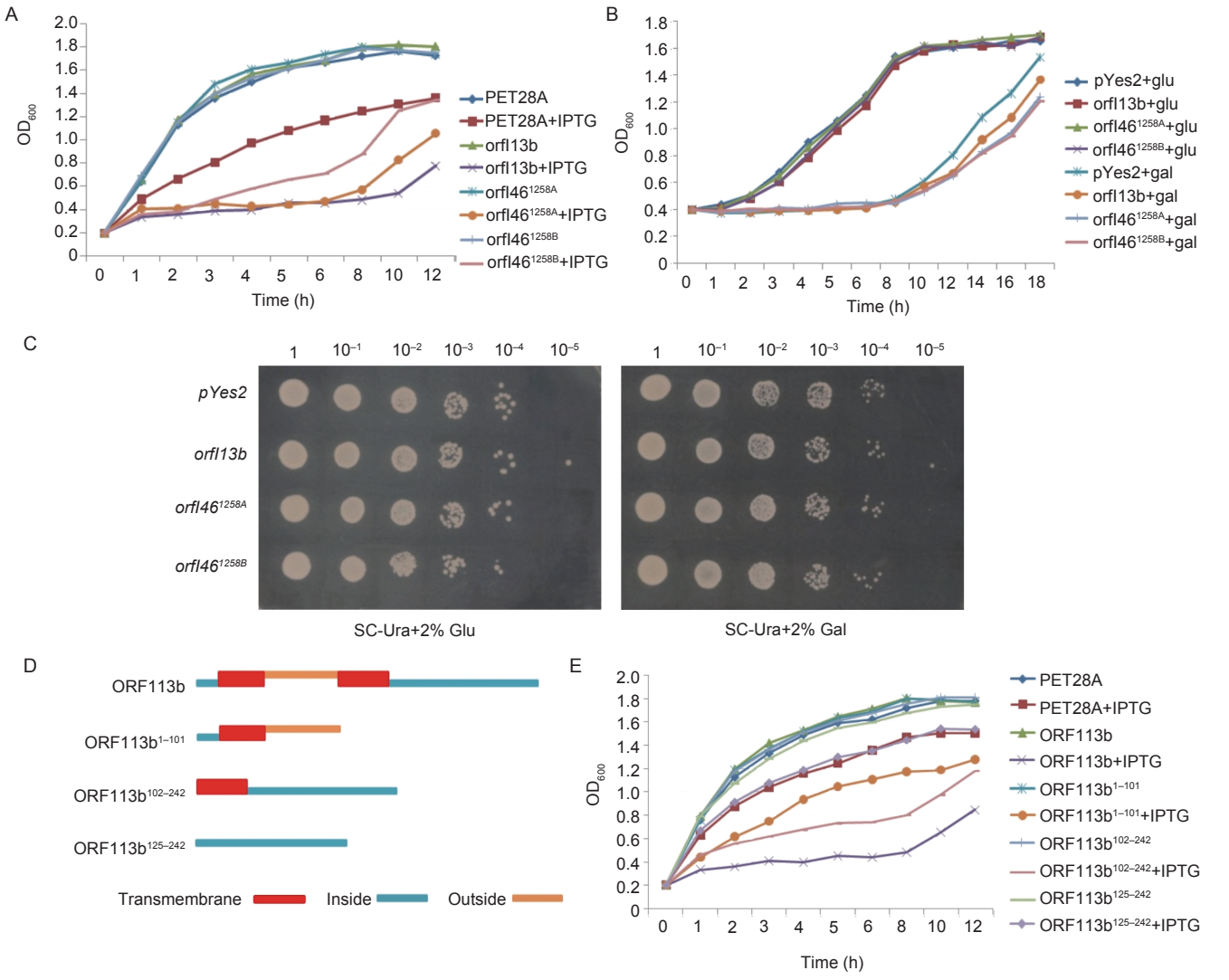


Fig. 4 Effects of *orf113b* and *orf146* expression on yeast and *Escherichia coli* (Rosetta) growth. A, growth curve of transformed *E. coli* in liquid medium. The *E. coli* single colonies containing *orf113b*, *orf146*, and the PET28A empty vector, were selected and shaken in 100 mL of Luria-Bertani (LB) liquid medium containing kanamycin. When the bacterial liquid OD_{600} reached 0.2, the sample was divided into two equal parts, with one getting isopropyl-β-D-thiogalactopyranoside (IPTG) to a final concentration of 1 mmol L^{-1}. The sample was then shaken and incubated at 37°C, with measurements of its OD value at intervals. B, growth curve of transformed yeast cells in liquid medium. Yeast single colonies containing the *orf113b*, *orf146*, and pYes2 vectors, were selected and shaken in 100 mL of synthetic complete-uraci (SC-Ura) liquid medium. When the OD_{600} reached 0.4, the sample was divided into two equal parts, with one getting 2% Glu, while the other received 2% Gal. The yeast culture was shaken and incubated at 29°C, with measurements of its OD value at intervals. C, growth of transformed yeast cells. The yeast was cultivated with the *orf113b*, *orf146*, and pYes2 vectors in SC-Ura liquid medium until OD_{600}=1. The medium was diluted to 1, 10^{-1}, 10^{-2}, 10^{-3}, 10^{-4}, and 10^{-5}, and added onto agar plates containing 2% Glu and 2% Gal. D, schematic diagram of the ORF113b truncated protein. The red line segment represents the transmembrane domain. E, induced expression of the truncated ORF113b fragment in *E. coli*.

Hydrogen peroxide effectively induces plant PCD by disrupting intracellular homeostasis. To simulate ROS stress in rapeseed seedlings, we applied exogenous H_2O_2 (20 mmol L^{-1}). Seedlings of the 1258B and 1258A lines were germinated in Petri dishes for 5 d, then transferred to dishes containing H_2O_2 (20 mmol L^{-1}) or distilled water as the controls. After 6 h, roots were harvested to assess mitochondrial gene expression and ATP content. The results revealed distinct OXPHOS gene expression patterns between 1258B and 1258A following ROS stress (Fig. 5-C and D). Specifically, in 1258B, genes in complex I (*nad1*, *nad5*, *nad6*, and *nad9*) and complex V (*atp1* and *atp9*) were significantly downregulated, whereas genes in complexes III and IV showed significant differences (Fig. 5-C). Conversely, in 1258A, complex I (*nad1*, *nad2*, *nad4*, and *nad5*), complex IV (*cox3*) and complex V (*atp1* and atp9) genes were significantly upregulated, while complex III (*cob*) was significantly downregulated (Fig. 5-C). Further analysis showed that after H_2O_2 stress, the expression of complex I genes (*nad1*, *nad2*, and *nad5*) in 1258A roots and anthers was significantly upregulated, while complex III (*cob*) and complex V (*atp6*) genes were significantly downregulated, with the complex IV gene (*cox3*) showing the opposite trends (Fig. 5-A and D). In addition, ATP content measurements showed that 1258A was more sensitive to H_2O_2 stress, exhibiting significantly lower ATP levels compared to 1258B under identical conditions (Fig. 5-E). These findings suggest that the *orf113b* and *orf146* genes may disrupt mitochondrial oxidative phosphorylation, leading to excessive ROS production and contributing to oxidative stress during 1258A anther development.

3.6. *orf113b* and *orf146* regulate pollen abortion in *A. thaliana*

To confirm the association of *orf113b* and *orf146* with pollen abortion, we cultivated transgenic *A. thaliana* lines expressing six different constructs: *AP3*::*MTS*:*orf113b*, *AP3*::*MTS*:*orf146*, *AP3*::*orf113b*, *AP3*::*orf146*, *35S*::*orf113b*, and *35S*::*orf146*. The anther-specific *APETALA3* (*AP3*) in *A. thaliana*, and the *CaMV35S* (*35S*) promoter, were utilized in these constructs. In addition, the mitochondrial targeting sequence (MTS) was derived from the first 165 bp of the fertility restoration gene *Rfo* (LOC108827691) from rapeseed *Ogu* CMS, and fused to the target gene following Sang *et al.* (2021). We observed pollen sterility in seven lines transformed with *AP3::MTS:orf113b*, eight lines with *AP3::MTS:orf146*, five lines with *AP3::orf113b*, six lines with *AP3::orf146*, five lines with *35S::orf113b*, and seven lines with *35S::orf146* (Appendix K). Overexpression of *orf113b* and *orf146* in *A. thaliana* clearly leads to pollen abortion, withered anthers, and the absence of pollen production (Fig. 6; Appendix L). Transgenic strains expressing *AP3*::*MTS*:*orf113b* and *AP3*::*MTS*:*orf146* exhibited severely impaired stamen

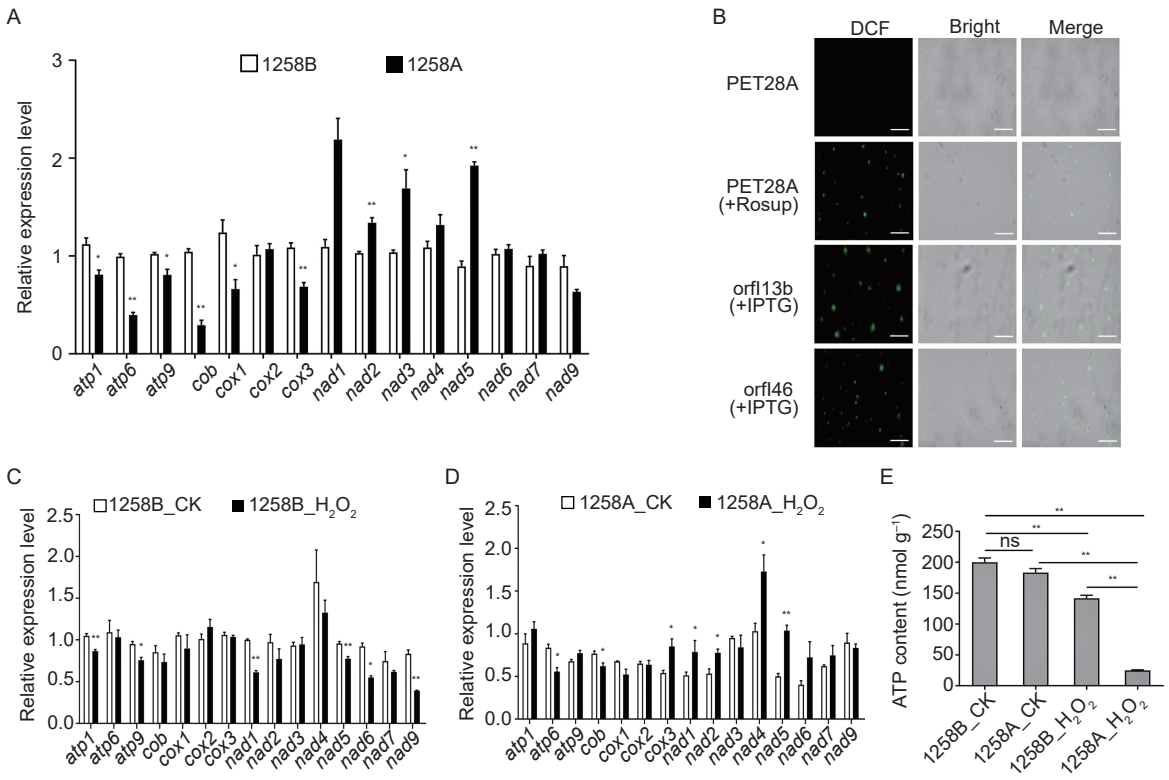


Fig. 5 Expression of genes in the mitochondrial oxidative phosphorylation pathway and reactive oxygen species (ROS) analysis. A, qRT-PCR results for genes in the mitochondrial oxidative phosphorylation (OXPHOS) pathway in the anthers of the sterile and maintainer lines. B, induced expression in *Escherichia coli* stimulates ROS production, with fluorescent 2′,7′-dichlorodihydrofluorescein (DCF) indicating ROS generation. Bar=50 μm. C and D, qRT-PCR results for genes in the mitochondrial OXPHOS pathway in the roots of the maintainer and sterile lines, respectively, after treatment with H_2O_2 (20 mmol L^{-1}) and CK (pure water). E, ATP content in seedlings. Bars mean SD (n=3). * and **, P<0.05 and P<0.01, respectively; ns, not significant, P>0.05.

development, characterized by shortened filaments (Fig. 6), whereas the other transgenic strains did not show significant stamen filament shortening (Appendix L). The ATP content in the flower buds of these transgenic lines was markedly lower than in the positive control, particularly in lines transformed with the *AP3::MTS:orf113b* and *AP3::MTS:orf146* vectors (Appendix M). In addition, we found abnormal expression of mitochondrial oxidative phosphorylation pathway genes in the transgenic lines (Appendix M). Notably, all three expression vectors induced pollen abortion in *A. thaliana* without affecting anther or filament formation. Although the flower structure remained unchanged, no pollen was produced, consistent with the 1258A pollen abortion phenotype (Xing *et al.* 2022).

3.7. Transcriptome data analysis of *orf113b* and *orf146* induced pollen abortion

The transgenic *A. thaliana* plants we cultivated consistently exhibited a pollen abortion phenotype, regardless of the transformation vectors used. Therefore, we speculated that *orf113b* and *orf146* share mechanisms that influence the transcriptional regulation of genes involved in anther development. Transcriptome analysis revealed that several of the top 10 significantly enriched GO terms were related to defense responses, including response to abiotic stimulus, response to light stimulus, response to radiation, response to chemical stimulus, response to organic substance, response to endogenous stimulus, response to hormone, and response to oxygen-containing compound (Fig. 7-A and B). Notably, numerous defense-related GO terms were significantly enriched across the transgenic plants transformed with various vector types. This indicates that the expression of *orf113b* and *orf146* triggers substances that induce a series of stress responses in *A. thaliana*. In the analysis of KEGG pathways, *orf113b* transgenic plants were involved in 14 pathways, including metabolic pathways, photosynthesis, and biosynthesis of secondary metabolites,

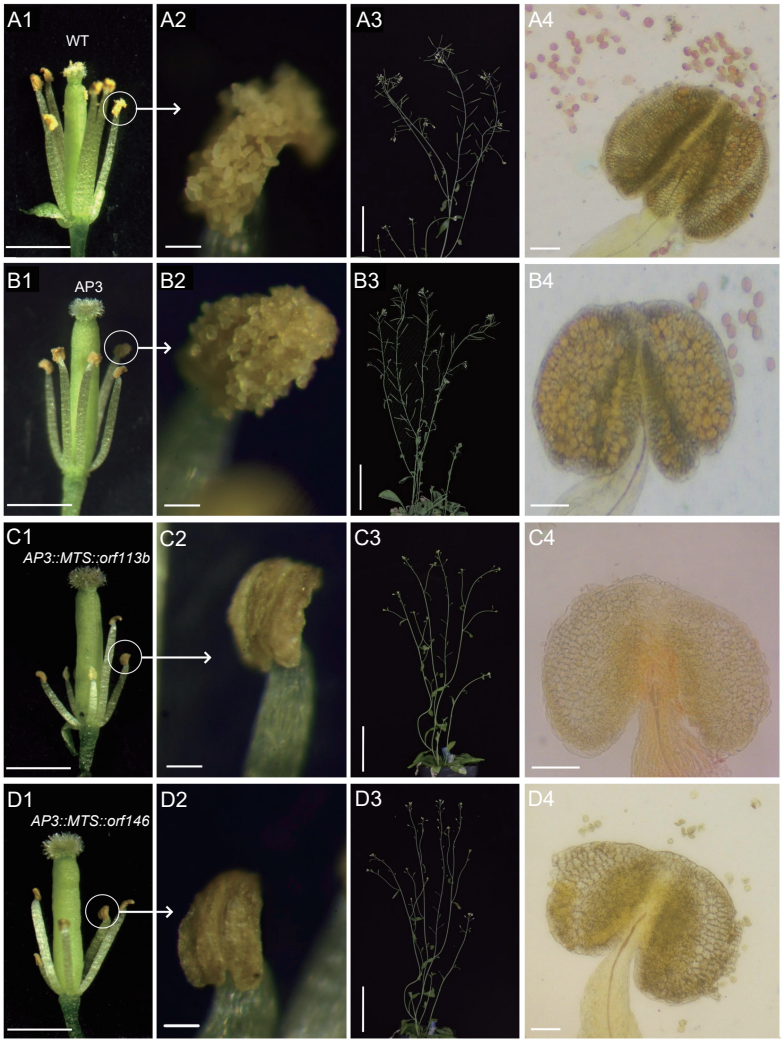


Fig. 6 Identification of transgenic plant phenotypes. A1–A4, phenotypes of wild-type *Arabidopsis thaliana* stamens, anthers, siliques, and pollen. B1–B4, phenotypes of *A. thaliana* stamens, anthers, siliques, and pollen carrying the *AP3* promoter vector. C1–C4, phenotypes of *A. thaliana* stamens, anthers, siliques, and pollen carrying the *AP3*::*MTS*:*orf113b* vector. D1–D4, phenotypes of *A. thaliana* stamens, anthers, siliques, and pollen carrying the *AP3*::*MTS*:*orf146* vector. In A1, B1, C1, and D1, the bar=1 mm; in A2, A4, B2, B4, C2, C4, D2, and D4, the bar=100 μm; and in A3, B3, C3, and D3, the bar=5 cm.

while *orf146* transgenic plants were significantly enriched in only three pathways: photosynthesis-antenna proteins, homogalacturonan degradation, and plant hormone signal transduction (Fig. 7-A and B). Given that the expression of both the *orf113b* and *orf146* genes can induce pollen abortion, we aimed to identify commonalities in the associated differential metabolic pathways. Differential gene analysis of three types of transgenic plants revealed 162 common differential genes in *orf113b* transgenic plants (Fig. 7-C) and 181 in *orf146* transgenic plants (Fig. 7-D). Subsequent KEGG enrichment analysis indicated that the differential genes in *orf113b* transgenic plants were predominantly enriched in biosynthesis of secondary metabolites, carotenoid biosynthesis, plant hormone signal transduction, metabolic pathways, oxidative phosphorylation, and the alanine, aspartate and glutamate metabolism pathways (Fig. 7-E). In contrast, the differential genes in *orf146* transgenic plants were significantly enriched in flavonoid biosynthesis, circadian rhythm — plant, and plant hormone signal transduction pathways (Fig. 7-F). Notably, the plant hormone signal transduction pathway was significantly enriched across both transgenic plant types.

Given the consistent pollen sterility observed in *orf113b* and *orf146* transgenic plants, we speculated that these two genes may target the same nuclear genes in *A. thaliana*, thereby inducing pollen sterility. To investigate the core regulatory genes involved in this sterility, we analyzed transcriptome sequencing data from the inflorescences of transgenic *A. thaliana* using gene co-expression analysis. We constructed a co-expression network comprising 83 genes, all of which exhibited positive correlations (Fig. 8-A). Focusing on the top 28 genes with more than 15 connections, we found that their expression levels were significantly higher in the transgenic lines compared to the wild type. Notably, 11 genes (*AT1G01980*, *AT1G55560*, *AT3G02810*, *AT3G09530*, *AT1G58120*, *AT5G50030*, *AT5G50830*, *AT2G26850*, *AT4G36490*, *AT1G04470*, and *AT5G18910*) showed significantly elevated expression levels across the three types of vector-transformed plants. Interestingly, in *35S*::*orf113b* transgenic plants, 27 genes were significantly different from the control, with 21 genes reaching highly significant levels. In contrast, only one gene in *35S*::*orf146* transgenic plants showed a significant difference from the control. In the *AP3*::*MTS*:*orf146* transgenic plants, 14 genes exhibited significantly higher expression levels compared to the control. Conversely, in the *AP3*::*MTS*:*orf113b* transgenic plants, only one gene showed significant variation from the control. No significant differences were found in their expression between the *AP3*::*orf146* transgenic plants and the control, whereas in the *AP3*::*orf113b* transgenic plants, 15 genes showed significant differences in expression compared to the control. These variations may be attributed to the vector type used or the tissue sampled, indicating that *orf113b* can influence the expression of core genes in *A. thaliana* through overexpression alone. In contrast, *orf146* requires precise mitochondrial targeting to function effectively. In summary, our findings suggest that both *orf113b* and *orf146* can activate the defense response in *A. thaliana*, leading to the significant upregulation of specific nuclear genes, potentially contributing to pollen sterility.

4. Discussion

4.1. Characteristics of high-quality mitochondrial genomes of 1258A and 1258B

We assembled the mitochondrial genomes of two alloplasmic cytoplasmic male sterility lines, 1258A and its maintainer line 1258B, both of which possess cytoplasm derived from a wild mustard species native to Xinjiang, known as Xinjiang wild rapeseed. The mitochondrial genome of 1258A spans 263,010 bp, while that of 1258B is slightly smaller at 262,916 bp (Fig. 1). Interestingly, the mitochondrial genome of 1258A exceeds that of *S. arvensis* (240,024 bp) in size, yet it remains 6,967 bp smaller than the previously reported *Nsa* CMS mitochondrial genome (Sang *et al.* 2019). The mitochondrial genome sizes of 1258A and 1258B differ by a mere 94 bp, suggesting minimal size variation. This similarity could be attributed to the lack of large repeated segments, as both the sterile and maintainer lines' mitochondrial genomes predominantly consist of small repeated fragments.

Mitochondrial genomes in sterile plant lines are typically larger than those in fertile lines, a difference often attributed to large repeated segments within the genomes of sterile lines. For example, the *Ogu* CMS mitochondrial genome is approximately 14 kb larger than its fertile counterpart (Tanaka *et al.* 2012), the *hau* CMS genome exceeds its maintainer line by 28 kb (Heng *et al.* 2014), and the *Nsa* CMS genome is 48 kb larger than that of its maintainer line (Christensen *et al.* 2021). Plant mitochondrial genomes are known for their rapid structural evolution but slow sequence evolution (Christensen *et al.* 2021; Wang *et al.* 2024). Studies on cotton have shown that expansions in mitochondrial genome size are mainly due to extensive sequence duplication and the insertion of sequences from distantly related species (Feng *et al.* 2023). These findings suggest that plant mitochondrial genomes evolve through sequence duplication-mediated recombination. Research on wild rice mitochondrial genes has further demonstrated their potential to evolve into functional CMS genes through multiple rearrangements, sequence variations, and the sub-stoichiometric shifting of conserved mitochondrial sequences (Tang *et al.* 2016). Despite the significant conservation of nucleotide sequences within syntenic regions across the 1258A, 1258B, and *S. arvensis* mitochondrial genomes, evolutionary rearrangements have altered the order and orientation of these regions. This suggests that the mitochondrial genomes of 1258A and 1258B may have undergone changes through repeat sequence-mediated recombination, which is associated with the emergence of new genes. Phylogenetic analysis indicates that the 1258A mitochondrial genome originated from wild mustard and shares a distant relationship with other CMS mitochondrial genomes found in rapeseed. This observation suggests that the 1258A mitochondrial genome predominantly retains the characteristics of the mitochondrial genome found in Xinjiang wild rapeseed.

4.2. Transmembrane domain is a fundamental characteristic of CMS proteins

Research shows that many CMS proteins are chimeric open reading frames (ORFs) that incorporate sequences from mitochondrial genes such as *cox*, *atp*, and *nad*, into

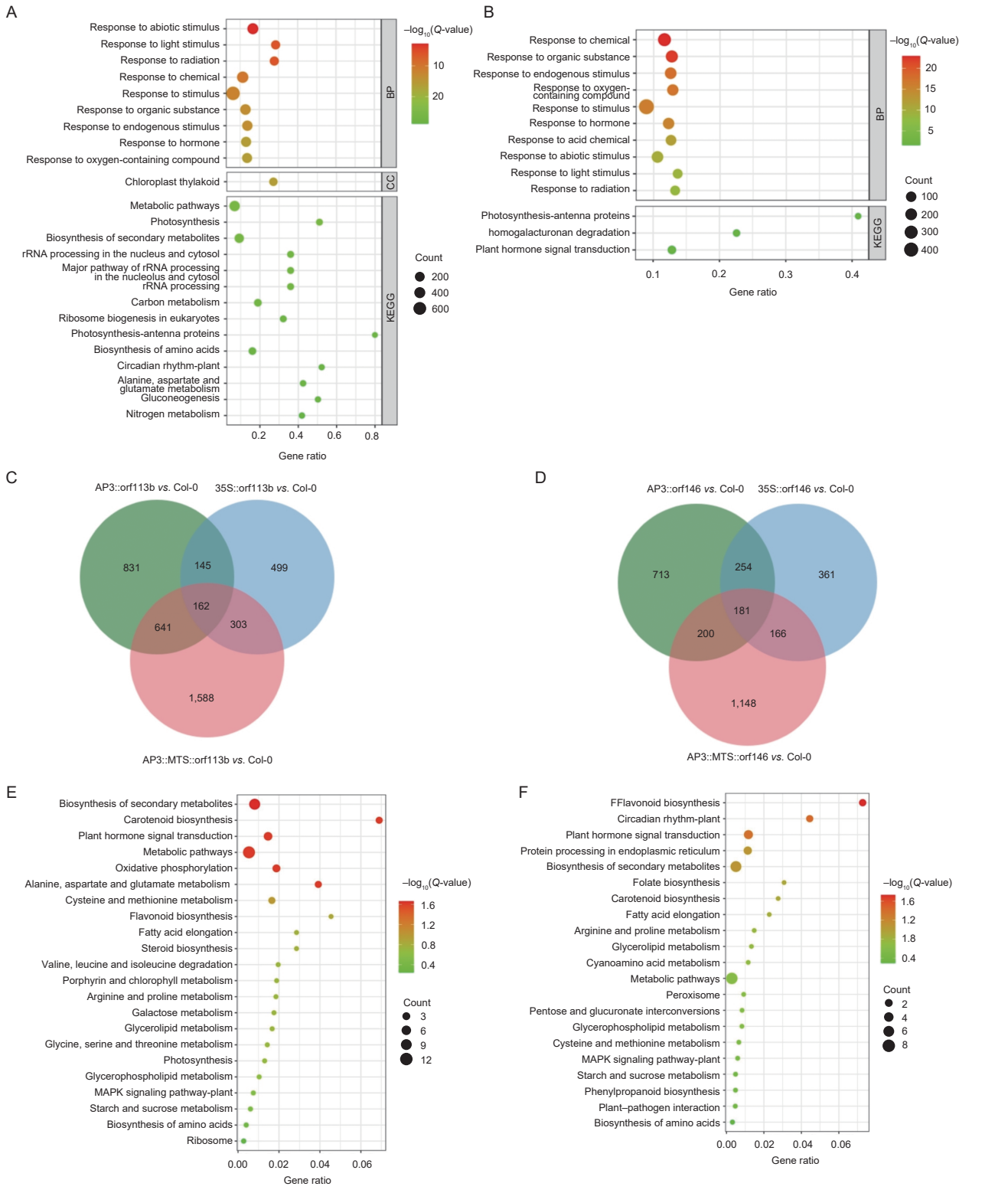


Fig. 7 Analysis of differentially expressed genes of the *orf113b* and *orf146* expressing *Arabidopsis thaliana* transgenic lines. A, Gene Ontology (GO) and Kyoto Encyclopedia of Genes and Genomes function (KEGG) enrichment analyses among genes in *orf113b* transgenic lines. B, GO and KEGG enrichment analyses among genes in *orf146* transgenic lines. C, numbers of differentially expressed genes and Venn diagrams between three *orf113b* lines. D, numbers of differentially expressed genes and Venn diagrams between three *orf146* transgenic lines. E, KEGG enrichment pathways of the core differentially expressed genes in *orf113b* transgenic lines. F, KEGG enrichment pathways of the core differentially expressed genes in *orf146* transgenic lines.

sterility genes (Chen and Liu 2014). For example, the CMS-HL gene in rice, *orfH79*, integrates a segment of the mitochondrial *cox2* gene (Liu *et al.* 2012). Similarly, the CMS gene *orf463* in radish is merged with *cox1* (Park *et al.* 2013). In sunflower and canola, the CMS genes *orfH522* (Köhler *et al.* 1991), *orf222* (*Nap* CMS), and *orf224* (*pol*

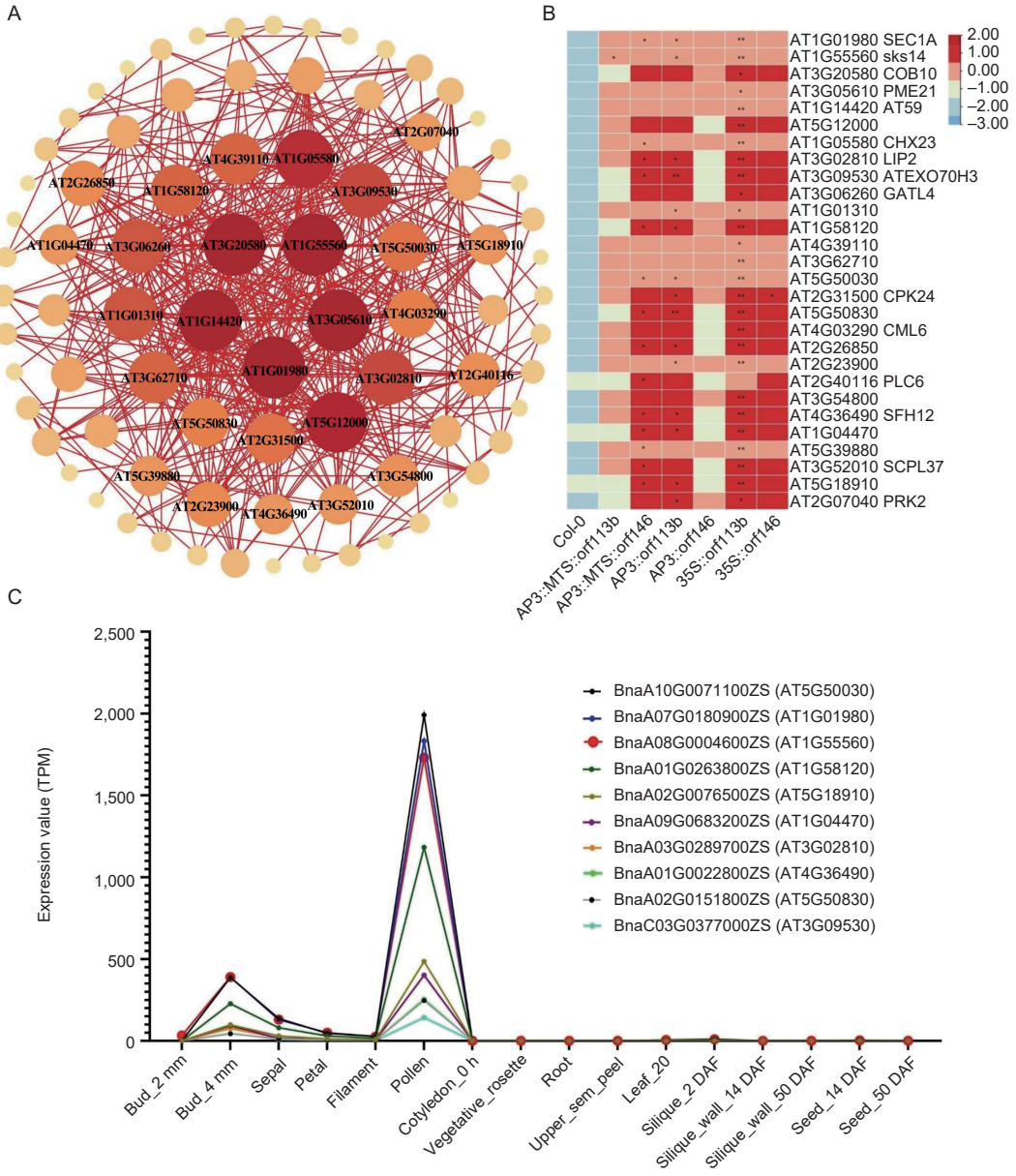


Fig. 8 Use of co-expression relationships to mine the core regulatory genes and their expression in ZS11 (*Brassica napus* L.). A, differential gene co-expression network diagram, where larger nodes indicate a greater number of connections to the node. Red lines indicate positive correlations. B, co-expression core gene clustering analysis for transgenic strains (log_2FC<0.5), with significance levels: *, P<0.05; **, P<0.01. C, expression patterns of *Arabidopsis thaliana* homologous genes in ZS11. DAF, days after flowering.

CMS) are fused with *atp8* (Handa *et al.* 1995; L'Homme *et al.* 1997). Moreover, CMS-related sterility genes in crops such as maize (Yang *et al.* 2022), cotton (Zhang *et al.* 2022), and pepper (Kim *et al.* 2007) have also been identified as fused with mitochondrial functional genes. Despite the frequent fusion of mitochondrial sequences in CMS sterility genes, there is no direct evidence that these fused genes are essential for the pollen sterility caused by CMS. For instance, in the *Ogu* CMS system, short mitochondrial repeats trigger extensive rearrangements between the fertile and sterile genomes, resulting in the sterility gene *orf138* (Singh *et al.* 2021). However, there is no evidence that *orf138* is a chimeric gene containing mitochondrial genes or sequences. In contrast, in the *Nsa* CMS system, the sterility gene *orf346* is co-transcribed with the *nad3* and *rpl12* genes (Sang *et al.* 2021), suggesting that chimeric structures are not universally present in CMS sterility genes.

The identification of all chimeric ORFs encoding transmembrane proteins in CMS highlights the transmembrane domain's pivotal role in plant CMS proteins. This domain is crucial for CMS sterility proteins not just structurally but also functionally. Studies using a prokaryotic expression system (*E. coli*) have shown that CMS proteins can directly impair bacterial viability and inhibit growth, a toxic function dependent on the presence of the transmembrane domain (Xiao *et al.* 2020; Sang *et al.* 2021). Similar findings have been reported in a eukaryotic expression system (yeast), where the toxicity

of CMS sterility proteins also relies on the transmembrane domain (Zhang *et al*. 2022). This study's truncated expression analysis of *Nsa* CMS proteins further supports that previous research by demonstrating that ORF113b's ability to inhibit bacterial growth is contingent on its transmembrane domain; without it, the protein loses this inhibitory function (Fig. 4). However, unlike earlier studies, our results show that ORF113b and ORF146 do not directly kill bacteria, but rather moderately restrict their proliferation. This inhibition is less potent than the toxicity observed with the ORF345 (Sang *et al.* 2021) and ORF610a (Zhang *et al.* 2022) proteins, suggesting variability in the degree of bacterial growth inhibition among different CMS sterility proteins.

4.3. *orf113b* and *orf146* are functional genes that regulate CMS pollen sterility

Our study demonstrates that the mitochondrial genes *orf113b* and *orf146* can induce pollen-free anther formation without altering floral organ morphology. This function is distinct from the sterility gene *orf346* in *Nsa* CMS, which, regardless of the mitochondrial targeting sequence, causes complete pollen sterility in *A. thaliana* and severely disrupts the development of petals and stamens, leading to significant floral organ abnormalities (Sang *et al.* 2021). Previous studies have documented that the expression of mitochondrial sterility genes in *A. thaliana* leads to compromised developmental phenotypes, such as partial pollen sterility, shortened siliques, reduced filament length, defective pollen tubes, and occasional partial fertility (Zhang *et al*. 2022). Importantly, our research identifies *orf113b* and *orf146* as key inducers of pollen sterility, with *orf113b* being unique to the sterile line 1258A. Conversely, the origin of *orf146* in 1258A was linked to base deletions and mutations within the gene (Fig. 3). Specifically, a 39 bp deletion in *orf146* reduces the transmembrane structural domains, altering both the amino acid sequences and types (Fig. 3-A). Single base mutations at positions 210, 320, and 324 bp in 1258A *orf146*, along with a base deletion at 315 bp, alter the amino acid sequence in this region, resulting in the loss of a transmembrane domain in 1258A ORF146 (Fig. 3-B). Recent studies using transcription activator-like effector nucleases (TALENs) to knockout the conserved mitochondrial *nad9* gene in tobacco have produced multiple deletion mutants of the mitochondrial *nad9* gene without inducing additional genomic rearrangements, thereby establishing a synthetic CMS system (Forner *et al.* 2023). These findings indicate that deletions and mutations in mitochondrial genes can induce CMS. Our results demonstrate that the redundant regulation of *orf113b* and *orf146* effectively ensures complete sterility in 1258A pollen but also complicates the development of restoration lines.

4.4. ROS signals regulate the expression of key nuclear genes to induce pollen abortion

The mitochondrial respiratory chain is the primary source of ROS in cells, especially through oxidative phosphorylation. This process not only produces over 90% of a cell's ATP but also generates significant amounts of ROS. Specifically, complexes I and III within the respiratory chain are the main sites of ROS production (Lanciano *et al.* 2013; Zorov *et al.* 2014). Among these, complex III is the major source of superoxide and other ROS derivatives. In our study, we observed abnormal expression patterns of functional genes related to the mitochondrial oxidative phosphorylation pathway in the anthers of sterile lines. Notably, genes *nad1*, *nad2*, *nad3*, and *nad5*, which are components of mitochondrial complex I, were significantly upregulated. Conversely, genes associated with complex III (*cob*), complex IV (*cox1* and *cox3*), and complex V (*atp1*, *atp6*, and *atp9*) were markedly downregulated (Fig. 5-A). These results indicate that ORF113b and ORF146 may influence the expression of genes in complexes I and III. In addition, we detected excessive ROS accumulation within cells, leading us to hypothesize that *orf113b* and *orf146* contribute to elevated ROS levels (Fig. 5-B). When oxidative stress was simulated in cells using H_2O_2 (Fig. 5-D), the expression patterns of genes from complex I (*nad1*, *nad2*, and *nad5*), complex III (*cob*), and complex V (*atp6*) in the roots of 1258A seedlings mirrored those observed in the anthers of 1258A. This consistency suggests a strong link between the oxidative stress experienced during pollen development in 1258A and the ROS generated by *orf113b* and *orf146*.

Numerous studies have demonstrated that CMS is closely related to a significant buildup of ROS within anthers. The maize CMS-C mitochondrial gene, *atp6c*, and the CMS-S mitochondrial gene, *orf355*, specifically trigger a surge in ROS levels, resulting in CMS in maize (Xiao *et al*. 2020; Yang *et al.* 2022). Similarly, pollen sterility in various CMS systems, including rice CMS-WA (Luo *et al.* 2013), CMS-HL (Wang *et al.* 2013), CMS-TA (Takatsuka *et al.* 2021), and others such as rapeseed *hau* CMS (Heng *et al*. 2018), *SaNa-1A* CMS (Du *et al*. 2019), *Ogu* CMS (Wang *et al.* 2021), and *Nsa* CMS (Sang *et al.* 2021), results from excessive ROS accumulation driven by mitochondrial sterility genes. Notably, these CMS systems display abnormal PCD of the tapetum during pollen sterility, emphasizing the critical role of timely tapetum PCD in pollen development. Research shows that ROS levels in anthers influence tapetum development and PCD. For example, TDF1 modulates ROS levels by regulating the ascorbic acid (AsA) content, balancing cell division and differentiation within the tapetum (Wu *et al.* 2023). In addition, BOTRYOID POLLEN 1 affects rice anther development by regulating ROS levels through UDP sugar homeostasis, which impacts tapetum cell PCD (Chen *et al.* 2023). Notably, ROS act as retrograde signals from mitochondria to the nucleus, thereby regulating nuclear gene expression. When mitochondrial function is impaired by internal or external factors, mitochondrial retrograde regulation (MRR) is triggered (Ng *et al.* 2014; Welchen *et al.* 2020). This process involves mitochondria communicating their functional status to the nucleus through largely unidentified signaling pathways, which facilitates the transcriptional regulation of responsive genes. Recent studies indicate that mitochondria-derived ROS are crucial initiators of mitochondrial retrograde signaling in *A. thaliana* (Khan *et al.* 2024). Our research demonstrated that *A. thaliana* transformed with the *orf113b* and *orf146* genes exhibited activated defense responses, likely associated

with ROS increases induced by the ORF113b and ORF146 proteins.

Research indicates that ROS produced in specific organelles, often associated with stress and defense mechanisms, may interact with hormonal functions (Ng *et al.* 2014; Xia *et al.* 2015; Liang *et al.* 2025). Our transcriptome data analysis revealed significant enrichment in the plant hormone signal transduction pathway (Fig. 7-E and F). Co-expression network analysis identified nuclear genes that are likely responsive to ROS signals, which are linked to pollen sterility (Fig. 8). Notably, these critical nuclear genes are upregulated. The gene *AT1G01980* encodes a reticuline oxidase-like protein involved in plant defense against pathogens, indicating a cellular stress response (Belchí-Navarro *et al.* 2013; Sabater-Jara *et al.* 2014). Furthermore, *AT1G55560* encodes the L-ascorbate oxidase homolog SKEWED5-SIMILAR 14 (SKS14). Ascorbate oxidase is reportedly crucial for regulating AsA levels, and disruption of SKS18 can increase AsA concentrations, thereby reducing ROS accumulation in tapetum cells. Conversely, SKS18 overexpression increases ROS levels in the tapetum, resulting in a larger cell volume and fewer tapetum cells (Wu *et al.* 2023). The protein kinase RBK2, encoded by *AT5G18910*, is mainly expressed during pollen development and is involved in oxidative stress signal transduction, cell wall biosynthesis, and ROS production (Molendijk *et al.* 2007). The high expression of these genes indicates that transgenic plant cells might suffer from ROS imbalance or exposure to toxic substances, adversely affecting tapetum cell function. However, the roles of the nuclear genes *AT1G58120*, *AT5G50030*, *AT5G50830*, *AT2G26850*, and *AT1G04470* remain unexplored. We hypothesize that these genes could respond to *orf113b* and *orf146* expression, potentially regulating ROS levels or influencing tapetal cell functions, which could affect pollen development. Validation of this hypothesis requires further comprehensive research.

Combining the current findings with our previous studies (Xing *et al.* 2022), we propose a model for the molecular regulatory mechanism of 1258A (*Nsa* CMS). The expression of mitochondrial genes *orf113b* and *orf146* impacts gene expression in the mitochondrial oxidative phosphorylation pathway, increasing mitochondrial ROS and reducing ATP levels. Elevated mitochondrial ROS can act as a retrograde signal to nuclear genes, thereby affecting pollen development and causing abnormal tapetal PCD and pollen sterility (Fig. 9).

5. Conclusion

The mitochondrial genome of 1258A (*Nsa* CMS), derived from Xinjiang wild rapeseed, is 263,010 bp long and includes three rRNAs, 19 tRNAs, 36 *orf* genes, and 33 protein-coding genes. Notably, the expression of the mutated and deleted gene *orf146* and the novel gene *orf113b* inhibits *E. coli* and yeast growth, disrupts mitochondrial oxidative phosphorylation gene expression, leads to ROS accumulation, and results in pollen abortion. Transcriptome analysis suggests that ROS produced by *orf146* and *orf113b* retrogradely regulate nuclear gene expression, thus impairing tapetum function and disrupting microspore development. Studying the molecular regulatory mechanism of CMS pollen abortion in 1258A will clarify the relevant nucleo-cytoplasmic interactions and aid in selecting restorer genes or lines.

Acknowledgements

This work was supported by the National Natural Science Foundation of China (3240150455), the China Agriculture Research System of MOF and MARA (CARS-13) and the National High-Tech R&D Program of China (863 Program, 2011AA10A104).

Declaration of competing interest

The authors declare that they have no conflict of interest.

Declaration of generative AI and AI-assisted technologies in the writing process

The authors declare that they did not use AI in the preparation and writing of this manuscript.

Appendices associated with this paper are available at https://doi.org/10.1016/j.jia.2024.09.018

References

Belchí-Navarro S, Almagro L, Sabater-Jara A B, Fernández-Pérez F, Bru R, Pedreño M A. 2013. Induction of trans-resveratrol and extracellular pathogenesis-related proteins in elicited suspension cultured cells of *Vitis vinifera* cv. Monastrell. *Journal of Plant Physiology*, **170**, 258–264.

Chase C D. 2007. Cytoplasmic male sterility: A window to the world of plant mitochondrial-nuclear interactions. *Trends in Genetics*, **23**, 81–90.

Chen H, Zhang S, Li R, Peng G, Chen W, Rautengarten C, Liu M, Zhu L, Xiao Y, Song F, Ni J, Huang J, Wu A, Liu Z, Zhuang C, Heazlewood J L, Xie Y, Chu Z, Zhou H. 2023. BOTRYOID POLLEN 1 regulates ROS-triggered PCD and pollen wall development by controlling UDP-sugar homeostasis in rice. *The Plant Cell*, **35**, 3522–3543.

Chen L, Liu Y G. 2014. Male sterility and fertility restoration in crops. *Annual Review of Plant Biology*, **65**, 579–606.

Christensen A C. 2021. Plant mitochondria are a riddle wrapped in a mystery inside an Enigma. *Journal of Molecular Evolution*, **89**, 151–156.

Dewey R E, Selote D, Griffin H C, Dickey A N, Jantz D, Smith J J, Matthiadis A, Strable J, Kestell C, Smith W A. 2023. Cytoplasmic male sterility and abortive seed traits generated through mitochondrial genome editing coupled with allotopic expression of atp1 in tobacco. *Frontiers in Plant Science*, **14**, 1253640.

Du K, Xiao Y, Liu Q, Wu X, Jiang J, Wu J, Fang Y, Xiang Y, Wang Y. 2019. Abnormal tapetum development and energy metabolism associated with sterility in SaNa-1A CMS of *Brassica napus* L. *Plant Cell Reports*, **38**, 545–558.

Eubel H, Heazlewood J L, Millar A H. 2006. *Isolation and Subfractionation of Plant Mitochondria for Proteomic Analysis*. Humana Press, Methods in Molecular Biology, USA. pp. 49–62.

Feng Y, Wang Y, Lu H, Li J, Akhter D, Liu F, Zhao T, Shen X, Li X, Whelan J, Zhang T, Hu J, Pan R. 2023. Assembly and phylogenomic analysis of cotton mitochondrial genomes provide insights into the history of cotton evolution. *The Crop Journal*, **11**, 1782–1792.

Forner J, Kleinschmidt D, Meyer E H, Gremmels J, Morbitzer R, Lahaye T, Schöttler M A, Bock R. 2023. Targeted knockout of a conserved plant mitochondrial gene by genome editing. *Nature Plants*, **9**, 1818–1831.

Ge X Y, Chen J L, Li O Q, Zou M, Tao B L, Zhao L, Wen J, Yi B, Tu J X, Shen J X. 2025. ORF138 causes abnormal lipid metabolism in the tapetum leading to Ogu cytoplasmic male sterility in *Brassica napus*. *Journal of Integrative Agriculture*, **24**, 2080–2095.

Guan C. 1996. Comparative studies of inheritable character in Xinjiang wild rape and *Sinapis arvensis* L. *Acta Agronomica Sinica*, **22**,

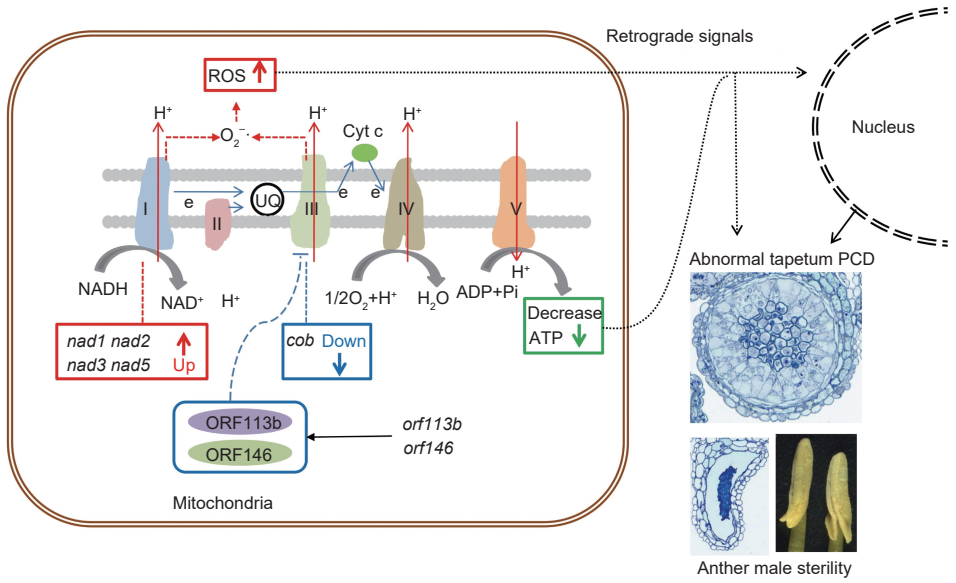


Fig. 9 A proposed working model for the possible male sterility mechanism in 1258A. ORF113b and ORF146 may cause dysfunction of complex III, thereby causing abnormal gene expression in the oxidative phosphorylation pathway, thus causing an reactive oxygen species (ROS) burst and reduced ATP production. Mitochondrial ROS and ATP can act as retrograde signals to nuclear genes, and jointly affect pollen development, thus resulting in abnormal tapetum programmed cell death (PCD) and pollen abortion.

214–219. (in Chinese)
Guan C, Yin M Z. 2014. Breeding of YeYou cytoplasmic male sterile line 1193A. In: *Proceedings of the Academic Annual Meeting of the Crop Science Society of China in 2014*. Nanjing, China. pp. 50–52. (in Chinese)
Handa H, Gualberto J M, Grienenberger J M. 1995. Characterization of the mitochondrial orfB gene and its derivative, *orf224*, a chimeric open reading frame specific to one mitochondrial genome of the "Polima" male-sterile cytoplasm in rapeseed (*Brassica napus* L.). *Current Genetics*, **28**, 546–552.
Heng S, Gao J, Wei C, Chen F, Li X, Wen J, Yi B, Ma C, Tu J, Fu T, Shen J. 2018. Transcript levels of *orf288* are associated with the hau cytoplasmic male sterility system and altered nuclear gene expression in *Brassica juncea*. *Journal of Experimental Botany*, **69**, 455–466.
Heng S, Wei C, Jing B, Wan Z, Wen J, Yi B, Ma C, Tu J, Fu T, Shen J. 2014. Comparative analysis of mitochondrial genomes between the *hau* cytoplasmic male sterility (CMS) line and its iso-nuclear maintainer line in *Brassica juncea* to reveal the origin of the CMS-associated gene *orf288*. *BMC Genomics*, **15**, 322.
Hu Q, Andersen S, Dixelius C, Hansen L. 2002. Production of fertile intergeneric somatic hybrids between *Brassica napus* and *Sinapis arvensis* for the enrichment of the rapeseed gene pool. *Plant Cell Reports*, **21**, 147–152.
Iwabuchi M, Koizuka N, Fujimoto H, Sakai T, Imamura J. 1999. Identification and expression of the kosena radish (*Raphanus sativus* cv. *Kosena*) homologue of the ogura radish CMS-associated gene, *orf138*. *Plant Molecular Biology*, **39**, 183–188.
Kazama T, Itabashi E, Fujii S, Nakamura T, Toriyama K. 2016. Mitochondrial ORF79 levels determine pollen abortion in cytoplasmic male sterile rice. *Plant Journal*, **85**, 707–716.
Khan K, Tran H C, Mansuroglu B, Önsell P, Buratti S, Schwarzländer M, Costa A, Rasmusson A G, Van Aken O. 2024. Mitochondria-derived reactive oxygen species are the likely primary trigger of mitochondrial retrograde signaling in *Arabidopsis*. *Current Biology*, **34**, 327–342.e4.
Kim D H, Kang J G, Kim B D. 2007. Isolation and characterization of the cytoplasmic male sterility-associated *orf456* gene of chili pepper (*Capsicum annuum* L.). *Plant Molecular Biology*, **63**, 519–532.
Köhler R H, Horn R, Lössl A, Zetsche K. 1991. Cytoplasmic male sterility in sunflower is correlated with the co-transcription of a new open reading frame with the *atpA* gene. *Molecular and General Genetics*, **227**, 369–376.
Kuwabara K, Arimura S I, Shirasawa K, Ariizumi T. 2022. *orf137* triggers cytoplasmic male sterility in tomato. *Plant Physiology*, **189**, 465–468.
Lanciano P, Khalfaoui-Hassani B, Selamoglu N, Ghelli A, Rugolo M, Daldal F. 2013. Molecular mechanisms of superoxide production by complex III: A bacterial versus human mitochondrial comparative case study. *Biochimica et Biophysica Acta*, **1827**, 1332–1339.
Landgren M, Zetterstrand M, Sundberg E, Glimelius K. 1996. Alloplasmic male-sterile Brassica lines containing *B. tournefortii* mitochondria express an ORF 3′ of the *atp6* gene and a 32 kDa protein. *Plant Molecular Biology*, **32**, 879–890.
L'Homme Y, Stahl R J, Li X Q, Hameed A, Brown G G. 1997. Brassica nap cytoplasmic male sterility is associated with expression of a mtDNA region containing a chimeric gene similar to the pol CMS-associated *orf224* gene. *Current Genetics*, **31**, 325–335.
Li P, Zhang D, Su T, Wang W, Yu Y, Zhao X, Li Z, Yu S, Zhang F. 2020. Genome-wide analysis of mRNA and lncRNA expression and mitochondrial genome sequencing provide insights into the mechanisms underlying a novel cytoplasmic male sterility system, BVRC-CMS96, in *Brassica rapa*. *Theoretical and Applied Genetics*, **133**, 2157–2170.
Liang Z M, Li J, Feng J Y, Li Z, Nangia V, Mo F, Liu Y. 2025. Brassinosteroids improve the redox state of wheat florets under low-nitrogen stress and alleviate degeneration. *Journal of Integrative Agriculture*, **24**, 2920–2939.
Liu G, Tian H, Huang Y Q, Hu J, Ji Y X, Li S Q, Feng Y Q, Guo L, Zhu Y G. 2012. Alterations of mitochondrial protein assembly and jasmonic acid biosynthesis pathway in Honglian (HL)-type cytoplasmic male sterility rice. *Journal of Biological Chemistry*, **287**, 40051–40060.
Liu J, Xiang R, Wang W, Mei D, Li Y, Mason A S, Fu L, Hu Q. 2015. Cytological and molecular analysis of *Nsa* CMS in *Brassica napus* L. *Euphytica*, **206**, 279–286.
Livak K J, Schmittgen T D. 2001. Analysis of relative gene expression data using real-time quantitative PCR and the $2^{-\Delta\Delta C_T}$ method. *Methods*, **25**, 402–408.
Luo D, Xu H, Liu Z, Guo J, Li H, Chen L, Fang C, Zhang Q, Bai M, Yao N, Wu H, Wu H, Ji C, Zheng H, Chen Y, Ye S, Li X, Zhao X, Li R, Liu Y G. 2013. A detrimental mitochondrial-nuclear interaction causes cytoplasmic male sterility in rice. *Nature Genetics*, **45**, 573–577.
Melonek J, Duarte J, Martin J, Beuf L, Murigneux A, Varenne P, Comadran J, Specel S, Levadoux S, Bernath-Levin K, Torney

F, Pichon J P, Perez P, Small I. 2021. The genetic basis of cytoplasmic male sterility and fertility restoration in wheat. *Nature Communications*, **12**, 1036.
Menassa R, L'Homme Y, Brown G G. 1999. Post-transcriptional and developmental regulation of a CMS-associated mitochondrial gene region by a nuclear restorer gene. *Plant Journal*, **17**, 491–499.
Mittler R, Zandalinas S I, Fichman Y, Van Breusegem F. 2022. Reactive oxygen species signalling in plant stress responses. *Nature Reviews Molecular Cell Biology*, **23**, 663–679.
Molendijk A J, Ruperti B, Singh M K, Dovzhenko A, Ditengou F A, Milia M, Westphal L, Rosahl S, Soellick T, Uhrig J, Weingarten L, Huber M, Palme K. 2007. A cysteine-rich receptor-like kinase NCRK and a pathogen-induced protein kinase RBK1 are Rop GTPase interactors. *Plant Journal*, **53**, 909–923.
Ng S, De Clercq I, Van Aken O, Law S R, Ivanova A, Willems P, Giraud E, Van Breusegem F, Whelan J. 2014. Anterograde and retrograde regulation of nuclear genes encoding mitochondrial proteins during growth, development, and stress. *Molecular Plant*, **7**, 1075–1093.
Nikornpun M, Sukwiwat K, Wongsing K, Kumchai J. 2023. Development of male sterile lines of CMS chilies (*Capsicum annuum* L.) from F_1 hybrids. *Breeding Science*, **73**, 158–167.
Park J Y, Lee Y P, Lee J, Choi B S, Kim S, Yang T J. 2013. Complete mitochondrial genome sequence and identification of a candidate gene responsible for cytoplasmic male sterility in radish (*Raphanus sativus* L.) containing DCGMS cytoplasm. *Theoretical and Applied Genetics*, **126**, 1763–1774.
Sabater-Jara A B, Almagro L, Pedreño M A. 2014. Induction of extracellular defense-related proteins in suspension cultured-cells of *Daucus carota* elicited with cyclodextrins and methyl jasmonate. *Plant Physiology and Biochemistry*, **77**, 133–139.
Sang S, Cheng H, Hao M, Ding B, Mei D, Wang H, Wang W, Liu J, Fu L, Liu K, Hu Q. 2021. Mitochondrial localization of ORF346 causes pollen abortion in alloplasmic male sterility. *The Crop Journal*, **9**, 1320–1329.
Sang S F, Mei D S. Liu J, Zaman Q U, Zhang H Y, Hao M Y, Fu L, Wang H, Cheng H T, Hu Q. 2019. Organelle genome composition and candidate gene identification for *Nsa* cytoplasmic male sterility in *Brassica napus*. *BMC Genomics*, **20**, 813.
Shinada T, Kikuchi Y, Fujimoto R, Kishitani S. 2006. An alloplasmic male-sterile line of *Brassica oleracea* harboring the mitochondria from Diplotaxis muralis expresses a novel chimeric open reading frame, *orf72*. *Plant & Cell Physiology*, **47**, 549–553.
Singh S, Bhatia R, Kumar R, Behera T K, Kumari K, Pramanik A, Ghemeray H, Sharma K, Bhattacharya R C, Dey S S. 2021. Elucidating mitochondrial DNA markers of ogura-based CMS lines in Indian cauliflowers (*Brassica oleracea* var. *botrytis* L.) and their floral abnormalities due to diversity in cytonuclear interactions. *Frontiers in Plant Science*, **12**, 631489.
Takatsuka A, Kazama T, Arimura S, Toriyama K. 2022. TALEN-mediated depletion of the mitochondrial gene *orf312* proves that it is a Tadukan-type cytoplasmic male sterility-causative gene in rice. *Plant Journal*, **110**, 994–1004.
Takatsuka A, Kazama T, Toriyama K. 2021. Cytoplasmic male sterility-associated mitochondrial gene *orf312* derived from rice (*Oryza sativa* L.) cultivar Tadukan. *Rice*, **14**, 46.
Tanaka Y, Tsuda M, Yasumoto K, Yamagishi H, Terachi T. 2012. A complete mitochondrial genome sequence of Ogura-type male-sterile cytoplasm and its comparative analysis with that of normal cytoplasm in radish (*Raphanus sativus* L.). *BMC Genomics*, **13**, 352.
Tang H, Zheng X, Li C, Xie X, Chen Y, Chen L, Zhao X, Zheng H, Zhou J, Ye S, Guo J, Liu Y G. 2016. Multi-step formation, evolution, and functionalization of new cytoplasmic male sterility genes in the plant mitochondrial genomes. *Cell Research*, **27**, 130–146.
Vercellino I, Sazanov L A. 2021. The assembly, regulation and function of the mitochondrial respiratory chain. *Nature Reviews. Molecular Cell Biology*, **23**, 141–161.
Wang C, Lezhneva L, Arnal N, Quadrado M, Mireau H. 2021. The radish Ogura fertility restorer impedes translation elongation along its cognate CMS-causing mRNA. *Proceedings of the National Academy of Sciences of the United States of America*, **118**, 35.
Wang H M, Ketela T, Keller W A, Gleddie S C, Brown G G. 1995. Genetic correlation of the *orf224/atp6* gene region with Polima CMS in *Brassica somatic* hybrids. *Plant Molecular Biology*, **27**, 801–807.
Wang J, Kan S, Liao X, Zhou J, Tembrock L R, Daniell, H, Jin S, Wu Z. 2024. Plant organellar genomes: Much done, much more to do. *Trends in Plant Science*, **29**, 754–769.
Wang K, Gao F, Ji Y, Liu Y, Dan Z, Yang P, Zhu Y, Li S. 2013. ORFH79 impairs mitochondrial function *via* interaction with a subunit of electron transport chain complex III in Honglian cytoplasmic male sterile rice. *New Phytologist*, **198**, 408–418.
Wang R, Ba Q, Zhang L, Wang W, Zhang P, Li G. 2022. Comparative analysis of mitochondrial genomes provides insights into the mechanisms underlying an S-type cytoplasmic male sterility (CMS) system in wheat (*Triticum aestivum* L.). *Functional & Integrative Genomics*, **22**, 951–964.
Wang R, Cai X, Hu S, Li Y, Fan Y, Tan S, Liu Q, Zhou W. 2020. Comparative analysis of the mitochondrial genomes of *Nicotiana tabacum*: Hints toward the key factors closely related to the cytoplasmic male sterility mechanism. *Frontiers in Genetics*, **11**, 257.
Welchen E, Canal M V, Gras D E, Gonzalez D H. 2020. Cross-talk between mitochondrial function, growth, and stress signalling pathways in plants. *Journal of Experimental Botany*, **72**, 4102–4118.
Wen J F, Zhao K, Lv J H, Huo J L, Wang Z R, Wan H J, Zhu H S, Zhang Z Q, Shao G F, Wang J, Zhang S, Yang T Y, Zhang J R, Zou X X, Deng M H. 2021. *Orf165* is associated with cytoplasmic male sterility in pepper. *Genetics and Molecular Biology*, **44**, e20210030.
Wu S Y, Hou L L, Zhu J, Wang Y C, Zheng Y L, Hou J Q, Yang Z N, Lou Y. 2023. Ascorbic acid-mediated reactive oxygen species homeostasis modulates the switch from tapetal cell division to cell differentiation in *Arabidopsis*. *The Plant Cell*, **35**, 1474–1495.
Xia X J, Zhou Y H, Shi K, Zhou J, Foyer C H, Yu J Q. 2015. Interplay between reactive oxygen species and hormones in the control of plant development and stress tolerance. *Journal of Experimental Botany*, **66**, 2839–2856.
Xiao S, Zang J, Pei Y, Liu J, Liu J, Song W, Shi Z, Su A, Zhao J, Chen H. 2020. Activation of mitochondrial *orf355* gene expression by a nuclear-encoded DREB transcription factor causes cytoplasmic male sterility in maize. *Molecular Plant*, **13**, 1270–1283.
Xing M, Guan C, Guan M. 2022. Comparative cytological and transcriptome analyses of anther development in *Nsa* cytoplasmic male sterile (1258A) and maintainer lines in *Brassica napus* produced by distant hybridization. *International Journal of Molecular Sciences*, **23**, 2004.
Yang H, Xue Y, Li B, Lin Y, Li H, Guo Z, Li W, Fu Z, Ding D, Tang J. 2022. The chimeric gene *atp6c* confers cytoplasmic male sterility in maize by impairing the assembly of the mitochondrial ATP synthase complex. *Molecular Plant*, **15**, 872–886.
Yang J, Liu X, Yang X, Zhang M. 2010. Mitochondrially-targeted expression of a cytoplasmic male sterility-associated *orf220* gene causes male sterility in *Brassica juncea*. *BMC Plant Biology*, **10**, 231.
You J, Li M, Li H, Bai Y, Zhu X, Kong X, Chen X, Zhou R. 2022. Integrated methylome and transcriptome analysis widen the knowledge of cytoplasmic male sterility in cotton (*Gossypium barbadense* L.). *Frontiers in Plant Science*, **13**, 770098.
Zhang J, Zhang L, Liang D, Yang Y, Geng B, Jing P, Qu Y, Huang J. 2023. ROS accumulation-induced tapetal PCD timing changes leads to microspore abortion in cotton CMS lines. *BMC Plant Biology*, **23**, 311.
Zhang Y, Han Y, Zhang M, Zhang X, Guo L, Qi T, Li Y, Feng J, Wang H, Tang H, Qiao X, Chen L, Song X, Xing C, Wu J. 2022. The cotton mitochondrial chimeric gene *orf610a* causes male sterility by disturbing the dynamic balance of ATP synthesis and ROS burst. *The Crop Journal*, **10**, 1683–1694.
Zorov D B, Juhaszova M, Sollott S J. 2014. Mitochondrial reactive oxygen species (ROS) and ROS-Induced ROS release. *Physiological Reviews*, **94**, 909–950.

Executive Editor-in-Chief Xueyong Zhang
Managing Editor Ning Wang